UPPSALA
UNIVERSITET

Digital Comprehensive Summaries of Uppsala Dissertations from the Faculty of Science and Technology 1562

Titan's ionosphere and dust

– as seen by a space weather station

OLEG SHEBANITS

ACTA
UNIVERSITATIS
UPSALIENSIS
UPPSALA
2017

ISSN 1651-6214
ISBN 978-91-513-0076-4
urn:nbn:se:uu:diva-329490

Dissertation presented at Uppsala University to be publicly examined in Ångström 2005, Lägerhyddsvägen 1, Uppsala, Friday, 3 November 2017 at 09:00 for the degree of Doctor of Philosophy. The examination will be conducted in English. Faculty examiner: Associate Professor Cesar Bertucci (Institute for Astronomy and Space Physics, COCICET/University of Buenos Aires, Buenos Aires, Argentina).

Abstract
Shebanits, O. 2017. Titan's ionosphere and dust. – as seen by a space weather station. *Digital Comprehensive Summaries of Uppsala Dissertations from the Faculty of Science and Technology* 1562. 69 pp. Uppsala: Acta Universitatis Upsaliensis. ISBN 978-91-513-0076-4.

Titan, the largest moon of Saturn, is the only known moon with a fully developed nitrogen-rich atmosphere, its ionosphere is detectable as high as 2200 km above its surface and hosts complex organic chemistry. Titan's atmosphere and ionosphere has striking similarities to current theories of these regions around Earth 3.5 billion years ago. The Cassini spacecraft has been in orbit around Saturn since 2004 and carries a wide range of instruments for investigating Titan's ionosphere, among them the Langmuir probe, a "space weather station", manufactured and operated by the Swedish Institute of Space Physics, Uppsala.

This thesis presents studies of positive ions, negative ions and negatively charged dust grains (also called aerosols) in Titan's ionosphere using the in-situ measurements by the Cassini Langmuir probe, supplemented by the data from particle mass spectrometers. One of the main results is the detection of significant (up to about 4000 cm-3) charge densities of heavy (up to about 13800 amu/charge) negative ions and dust grains in Titan's ionosphere below 1400 km altitude. The dust is found to be the main negative charge carrier below about 1100 km on the nightside/terminator ionosphere, forming a dusty plasma (also called "ion-ion" plasma). A new analysis method is developed using a combination of simultaneous observations by multiple instruments for a case study of four flybys of Titan's ionosphere, further constraining the ionospheric plasma charge densities. This allows to predict a dusty plasma in the dayside ionosphere below 900 km altitude (thus declaring it a global phenomenon), as well as to empirically estimate the average charge of the negative ions and dust grains to between -2.5 and -1.5 elementary charges. The complete Cassini dataset spans just above 13 years, allowing to study effects of the solar activity on Titan's ionosphere. From solar minimum to maximum, the increase in the solar EUV flux increases the densities by a factor of ~2 in the dayside ionosphere and, surprisingly, decreases by a factor of ~3-4 in the nightside ionosphere. The latter is proposed to be an effect of the ionospheric photochemistry modified by higher solar EUV flux. Modelling photoionization also reveals an EUV trend (as well as solar zenith angle and corotational plasma ram dependencies) in the loss rate coefficient.

Keywords: Titan, Cassini, Ionosphere, Dusty plasma, Ion-ion plasma, Langmuir probe, aerosols, tholins

Oleg Shebanits, Swedish Institute of Space Physics, Uppsala Division, Box 537, Uppsala University, SE-75121 Uppsala, Sweden. Department of Physics and Astronomy, Space Plasma Physics, 516, Uppsala University, SE-751 20 Uppsala, Sweden.

ISSN 1651-6214
ISBN 978-91-513-0076-4
urn:nbn:se:uu:diva-329490 (http://urn.kb.se/resolve?urn=urn:nbn:se:uu:diva-329490)

– To my son Robert

List of Papers

This thesis is based on the following papers, which are referred to in the text by their Roman numerals.

I **Shebanits O.**, Wahlund J.-E., Mandt K.E., Ågren K., Edberg N.J.T., and Waite J.H. (2013), Negative ion densities in the ionosphere of Titan–Cassini RPWS/LP results, *Planetary and Space Science*, 84, 153–162, doi:10.1016/j.pss.2013.05.021.

II **Shebanits O.**, Wahlund J.-E., Edberg N.J.T., Crary F.J., Wellbrock A., Andrews D. J., Vigren E., Desai R.T., Coates A.J., Mandt K.E., Waite J.H. (2016), Ion and aerosol precursor densities in Titan's ionosphere: A multi-instrument case study, *Journal of Geophysical Research: Space Physics*, 121(10), 10,075-10,090, doi:10.1002/2016JA022980.

III **Shebanits O.**, Vigren E., Wahlund J.-E., Holmberg M.K.G., Morooka M., Edberg N.J.T., Mandt K.E., Waite J.H. (2017), Titan's ionosphere: a survey of solar EUV influences, *Journal of Geophysical Research: Space Physics*, 122, doi:10.1002/2017JA023987.

IV **Shebanits O.**, Vigren E., Wahlund J.-E., Edberg N.J.T., Cui J., Galand, M., Mandt K.E., Waite J.H., Photoionization modelling of Titan's dayside ionosphere, *The Astrophysical Journal Letters*, manuscript in preparation

Papers not included in the thesis

Edberg N.J.T., Andrews D.J., **Shebanits O.**, Ågren K., Wahlund J.-E., Opgenoorth H.J., Cravens T.E., Girazian Z. (2013a), Solar cycle modulation of Titan's ionosphere, *Journal of Geophysical Research: Space Physics*, 118(8), 5255–5264, doi:10.1002/jgra.50463.

Edberg N.J.T., Andrews D.J., **Shebanits O.**, Agren K., Wahlund J.-E., Opgenoorth H.J., Roussos E., Garnier P., Cravens T.E., Badman S.V., Modolo R., Bertucci C., Dougherty,M.K. (2013b), Extreme densities in Titan's ionosphere during the T85 magnetosheath encounter. *Geophysical Research Letters*, 40(12), 2879–2883, doi:10.1002/grl.50579.

Edberg N. J. T., Andrews D.J., Bertucci C., Gurnett D.A., Holmberg M.K.G., Jackman C.M., Kurth W.S., Menietti J.D., Opgenoorth H.J., **Shebanits O.**, Vigren E., Wahlund J.-E., (2015), Effects of Saturn's magnetospheric dynamics on Titan's ionosphere, *Journal of Geophysical Research: Space Physics*, 120(10), 8884–8898, doi:10.1002/2015JA021373.

Vigren E., Galand M., **Shebanits O.**, Wahlund J.-E., Geppert W.D., Lavvas P., Vuitton V., Yelle R.V. (2014a), Increasing Positive Ion Number Densities Below the Peak of Ion-Electron Pair Production in Titan's Ionosphere, *The Astrophysical Journal,* 786(1), 69, doi:10.1088/0004-637X/786/1/69.

Vigren E., Galand M., Yelle R.V., Wellbrock A., Coates A.J., Snowden D., Cui J., Lavvas P., Edberg N.J.T., **Shebanits O.**, Wahlund J.-E., Vuitton V., Mandt K.E. (2014b), Ionization balance in Titan's nightside ionosphere, *Icarus*, 248, 539–546, doi:10.1016/j.icarus.2014.11.012.

Desai R. T., Coates A. J., Wellbrock A., Vuitton V., Crary F. J., Caniulef D. G., **Shebanits O.**, Jones G. H., Lewis G. R., Waite J. H., Taylor S. A., Kataria D. O., Wahlund J.-E., Edberg N. J. T., and Sittler E. C. (2017), Carbon chain anions and the growth of complex organic molecules in Titan's ionosphere, *The Astrophysical Journal Letters*, 844(2), L18, doi:10.3847/2041-8213/aa7851.

Holmberg M.K.G., **Shebanits O.**, Wahlund J.-E., Morooka M. W., André N., Garnier P., Density structures, dynamics, and seasonal and solar cycle modulations of Saturn's inner plasma disk, submitted to *Journal of Geophysical Research: Space Physics*, under review.

Contents

Abbreviations

ASI	**A**genzia **S**paziale **I**taliana, Italian Space Agency
CAPS	**Ca**ssini **P**lasma **S**pectrometer
DC	**D**irect **C**urrent
ELS	**El**ectron **S**pectrometer
ENA	**E**nergetic **N**eutral **A**tom
ESA	**E**uropean **S**pace **A**gency
EUV	**E**xtreme **U**ltra-**V**iolet
HCOM	**H**eavy **C**omplex **O**rganic **M**olecule
IBS	**I**on **B**eam **S**pectrometer
INMS	**I**on and **N**eutral **M**ass **S**pectrometer
JPL	**J**et **P**ropulsion **L**aboratory (NASA)
JUICE	**Ju**piter **Ic**y Moons **E**xplorer
LP	**L**angmuir **P**robe
LT	(Titan) **L**ocal **T**ime
MSSL	**M**ullard **S**pace **S**cience **L**aboratory
NASA	**N**ational **A**eronautics and **S**pace **A**dministration
OML	**O**rbital **M**otion **L**imited theory
PAH	**P**olycyclic **A**romatic **H**ydrocarbon
RPWS	**R**adio and **P**lasma **W**ave **S**cience
SEE	**S**olar **E**UV **E**xperiment
SLT	**S**aturn **L**ocal **T**ime
SOLSTICE	**Sol**ar **St**ellar **I**rradiance **C**omparison **E**xperiment
SORCE	**So**lar **R**adiation and **C**limate **E**xperiment
SSL	**S**ub-**S**olar **L**atitude

SZA	**S**olar **Z**enith **A**ngle
SWRI	**S**outh**w**est **R**esearch **I**nstitute
TIMED	**T**hermosphere **I**onosphere **M**esosphere **E**nergetics and **D**ynamics

1 Introduction

The Saturnian system is a miniature model of a solar system. The interaction of its magnetospheric plasma with the numerous moons resembles that of solar wind and planets. The rings, full of particles and dust, offer insights into physics of protoplanetary disks and planetoid formation. Two of its moons, Titan and Enceladus, are candidates for extra-terrestrial life and may push our definitions of habitability.

Since the robotic exploration of the solar system has reached Saturn in 1979 (Pioneer 11 spacecraft, **Figure 1**), the giant planet itself and its satellites in particular have challenged scientists with unexpected physics. Titan, the largest companion of Saturn, has relinquished its mantle of the largest moon in the solar system with the arrival of the Voyager I spacecraft in 1980. It turned out that much of Titan's visual size is in fact due to its fluffy and hazy atmosphere, the radius of the moon being 2575 km.

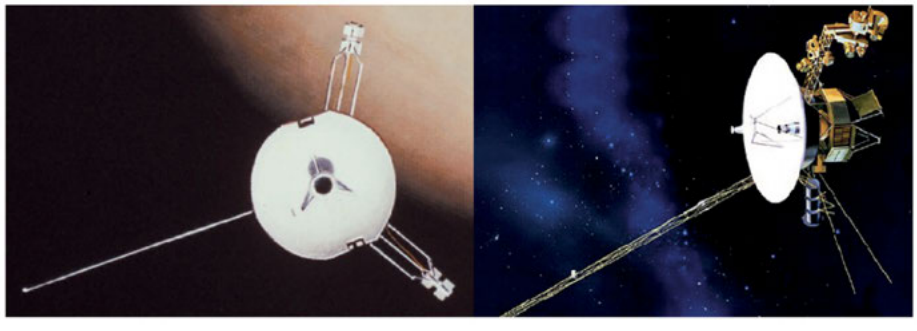

Figure 1. *Artist impressions of the Pioneer 11* ***(left)*** *and the Voyager 1* ***(right)*** *spacecraft*[1].

Voyager I was also the first to detect Titan's ionosphere during the first targeted flyby of the moon, coming as close as 2.7 Titan radii [Bird et al., 1997]. With a single flyby, the knowledge of the composition of the atmosphere and ionosphere was very limited [Coustenis et al., 2010; Cravens et al., 2010 and references therein]. Laboratory experiments suggested the

[1] Source: https://www.nasa.gov/centers/ames/news/2013/pioneer11-40-years.html and http://voyager.jpl.nasa.gov/multimedia/flash_html.html respectively

tholins[2] in Titan's signature orange haze to form from the chemically "close relatives" of methane- and nitrogen-like polycyclic aromatic hydrocarbons (PAHs[3], relatively simple molecules) and nitriles in the atmosphere around altitudes of few hundred kilometres, where the haze layers were observed by the Voyager [*Sagan et al.*, 1993; *Thompson et al.*, 1994].

The Cassini-Huygens spacecraft took a closer look at the giant planet (**Figure 2**), with specific objectives to study Saturn and Titan. Presently, Titan has been a topic of scientific scrutiny by the Cassini teams for over a decade and is presently known as the second largest moon in the solar system, the only one with a fully developed dense atmosphere ($\approx$ 150 kPa at the surface with the temperature of $\approx$ 94 K, *Fulchignoni et al.*, 2005) consisting mainly of nitrogen and methane (97% and $<$ 2.7% respectively, *Niemann et al.*, 2005; *Coustenis et al.*, 2007; *Waite et al.*, 2007s) and an ionosphere, hosting complex organic chemistry. Titan's ionosphere has been measured as far as ~2200 km above its surface (nearly a whole radius of the moon!), the ionopause[4] at a specific point depends on a lot of parameters however, and may fluctuate from flyby to flyby between ~1000 km (e.g., when Saturn's magnetopause is pushed past Titan and the moon is in shocked solar wind) and ~5000 km altitude (e.g., in Titan's corotational plasma wake) [e.g., *Wahlund*, 2005; *Garnier et al.*, 2009; *Edberg et al.*, 2010].

Figure 2. *Artist's impression of the Cassini-Huygens in orbit around Saturn (source: https://www.jpl.nasa.gov/missionspacecraftassini-huygens/).*

It was found that the PAHs and similar hydrocarbons, as well as nitriles, are forming already in the ionosphere [*Waite et al.*, 2007]. At the same time, the negative ions were discovered by the *in-situ* CAPS/ELS[5] measurements

[2] From Greek "θόλος" meaning "muddy", introduced by *Sagan and Khare*, 1979.

[3] **P**olycyclic **A**romatic **H**ydrocarbon

[4] Physical border of an ionosphere where its magnetic pressure balances the ambient one.

[5] **Ca**ssini **P**lasma **S**cience **El**ectron **S**pectrometer

[*Coates et al.*, 2007] with subsequent detection by the *in-situ* RPWS/LP[6] measurements [*Ågren et al.*, 2012; Paper I]. Due to the extreme mass/charge ratios (up to 13800 amu/q), the negative ions were gradually accepted as suitable candidates for aerosol/tholin precursors.

Thus the observations of positive and negative ions [*Wahlund*, 2005; *Waite et al.*, 2007; *Crary et al.*, 2009; *Sittler et al.*, 2009; *Wahlund et al.*, 2009b; *Coates et al.*, 2010a] and the chemical models based on measurements [e.g., *Vuitton et al.*, 2009, 2014 and references therein] have led the scientific consensus towards an idea (summarized in **Figure 3**) that the ionization of the atmosphere initiates a complex organic chemistry in the top layers of the ionosphere (∼1600 km altitude); the ions gradually grow and precipitate, forming aerosol precursors already in the lower ionosphere around ∼1000 km altitude.

This concept has roots in the famous Miller-Urey experiment, which showed a formation of amino acids in a gas mixture of nitrogen, methane and water vapor [*Miller*, 1953]. Modern (Cassini era) simulations of a Titan-like atmosphere reproduced tholins [*Gudipati et al.*, 2013] and amino acids from a waterless gas mixture of nitrogen, methane and carbon oxide [e.g., *Hörst et al.*, 2012].

With its fluffy nitrogen-rich atmosphere, Titan has been compared to Earth ∼3.5 Gyrs ago [e.g., *Pavlov et al.*, 2003; *Tian et al.*, 2008]. Models suggest that the early Earth, subjected to much stronger solar wind and EUV flux of a young Sun, also had extensive ionosphere [*Tian et al.*, 2008]. Combined with a weaker magnetosphere [*Tarduno et al.*, 2010], the conditions are analogous to Titan and its induced magnetosphere in Kronian[7] magnetospheric plasma flow. Another similarity is the presence of bodies of liquid on the surface – methane lakes in Titan's case [e.g., *Aharonson et al.*, 2014 and references therein]. With respect to composition, Titan's atmosphere has very limited supply of water[8] compared to early Earth – water group particles originate in Enceladus' plume [e.g., *Coates et al.*, 2010b; *Morooka et al.*, 2011; *Hill et al.*, 2012] and may be delivered to Titan's atmosphere via Saturn's magnetosphere [*Sittler et al.*, 2009]. Both environments seem to have the formation of the aerosols/tholins in the ionosphere [e.g., *Raulin et al.*, 2009 and references therein]. In light of this analogy and the tholin formation, the complex organic chemistry on Titan may shed light on the origins of life on Earth. This brings us to the overarching scientific interest of this thesis: production of complex

[6] **R**adio and **P**lasma **W**ave **S**cience **L**angmuir **P**robe

[7] Kronian ≡ Saturnian, from *Κρόνος*, the Greek name of Saturn

[8] Note: while water in the atmosphere of Titan is scarce, the moon does have a subsurface ocean [*Béghin et al.*, 2010]

organic molecules and particles in the atmosphere of Titan with implications for pre-biotic chemistry of early Earth. We approach the topic from the perspective of space physics, focusing on the plasma densities derived from the *in-situ* measurements by the Cassini spacecraft.

The outline of this thesis is as follows: Section 2 provides a brief description of the space environment (2.2), its effects on the spacecraft (2.3), and the relevant instruments with the corresponding measurement techniques (2.4). Section 3 gives an overview of Titan's ionosphere in light of the included papers and relevant discoveries: the origin (3.1), the bulk ionosphere as seen by the *in-situ* measurements (3.2) and the lower region populated by

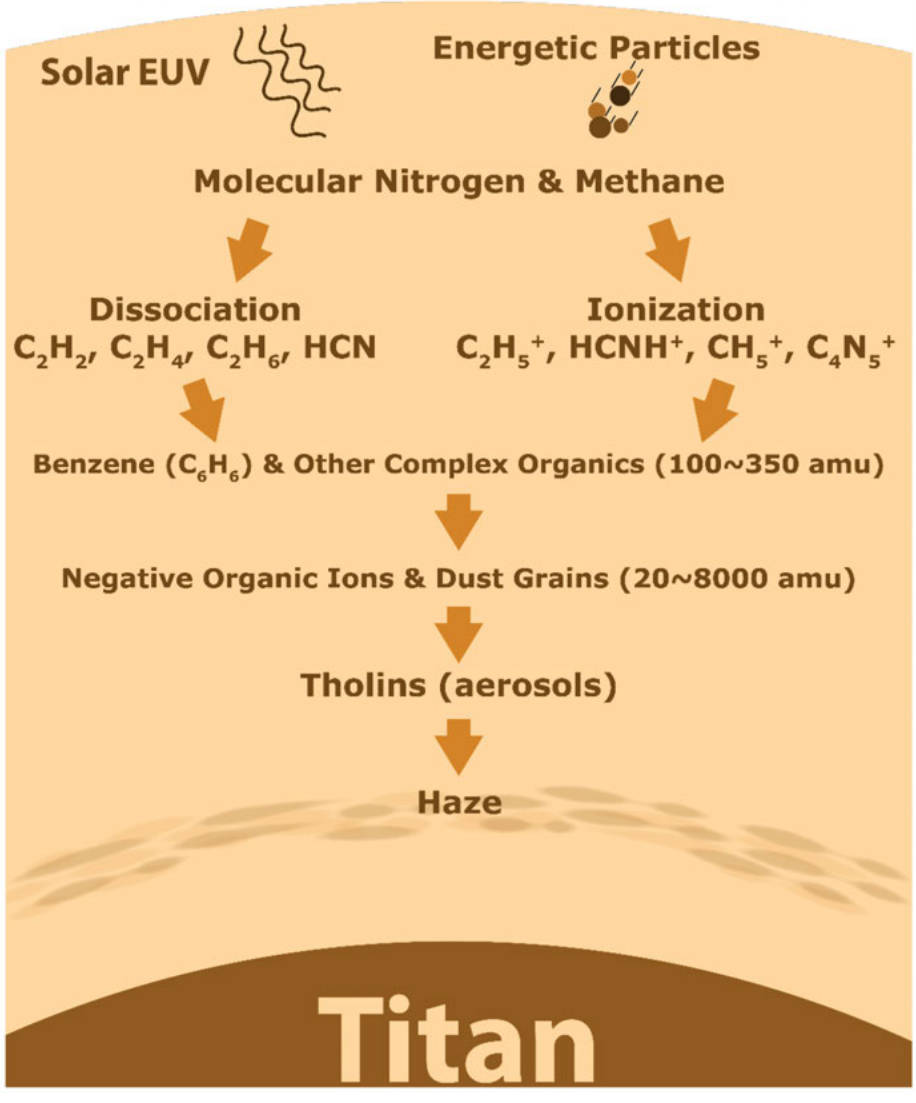

Figure 3. *Schematic of the tholin formation at Titan. Adapted from Waite et al., 2007.*

dust (3.3). Section 4 summarizes the included papers, followed by the list of cited literature.

This thesis is partly based on my licentiate thesis “Pre-biotic molecules and dynamics in the ionosphere of Titan”. All figures are used with permissions from the respective publishers.

2 Measurements

Spacecraft with their numerous instruments are our eyes and ears (and sometimes fingers) in the space and planetary exploration. Before we dive into the details of Titan's ionosphere, a brief overview of the setting, hardware, and measurement techniques is necessary.

2.1 Cassini-Huygens

The Cassini-Huygens is a joint ESA/NASA/ASI[9] mission, named after the astronomers Giovanni D. Cassini ($1625 - 1712$) and Christiaan Huygens ($1629 - 1695$), discoverers of Saturn's largest moons. The spacecraft launched in 1997, measuring 6.8×4 meters and weighing 5.82 tonnes (out of which 3.1 tonnes was propellant and only 49 kg were scientific instruments), and reached Saturn in 2004. After the ESA-built Huygens probe has been launched from the "mothercraft" Cassini and subsequently landed on Titan in January 2005, the mission is referred to simply as "Cassini". The mission was extended in 2008 under the name "Cassini Equinox mission" and again in 2010 as "Cassini Solstice Mission", setting the end of mission to September 2017 with a plan to terminate quite literally in a blaze of glory as it plunges into Saturn (fittingly named the "Cassini Grand Finale"). After these almost 20 years in space including 13 heavy-duty years in orbit around Saturn, the spacecraft and most of the instruments have been functioning until the very end[10].

[9] **E**uropean **S**pace **A**gency, **N**ational **A**eronautics and **S**pace **A**dministration and **A**genzia **S**paziale **I**taliana, the Italian Space Agency.

[10] The loss of contact occurred at 10:55 UTC on September 15th, 2017

2.2 Space environment

2.2.1 Plasma

Describing any topic of the space exploration is typically impossible without mentioning plasma. Fourth state of matter, plasma has been discussed as early as 1870s, although it was first called "radiant matter" due to its discovery in an electrical discharge tube, the embryo of the first television sets. Incidentally, while people were/are unaware of the fourth state of matter, it has been so to speak staring us right in the face long before the popularization of television, in the form of lightning and the northern lights. The term "plasma" was introduced in 1928 for a quasi-neutral[11] ionized gas [*Tonks and Langmuir*, 1929], a somewhat unfortunate naming as it is often confused with the blood plasma (coined a decade earlier). Plasma is the natural state of ~99% of visible matter in the known universe [see e.g., *Goldston and Rutherford*, 1995] and can be found in the interstellar and interplanetary media, nebulae, atmospheres of stars, planets and moons, cometary comas – in short, any gas in presence of any ionization source(s).

Plasma is characterized by its collective behaviour and quasi-neutrality, as well as its primary physical properties: electron and ion temperatures, charge densities and velocities. The collective behaviour is due to the electromagnetic interactions between the charged particles: each particle in a plasma is affected by (coupled to) many particles around it. At sufficiently low temperatures (or strong enough coupling) these interactions sets up a crystalline structure much like those in metals, although this never happens in a typical space and atmospheric environment. Quasi-neutrality is essentially a criterion that allows to discard the boundary effects in a plasma. Both of these characteristics are defined by a maximum distance over which each charged particle "feels" the others, called Debye length (λ_D) (or, more universally, screening length)[12]. For the collective behaviour to occur, the charged particles have to be no farther than one Debye length of each other (and there has to be many particles within a "Debye sphere"); for the quasi-neutrality to apply, the Debye length has to be much smaller than the physical size of the plasma.

[11] *quasi-neutrality*: approximately (sufficiently) equal amounts of positive and negative charge carriers

[12] the Debye (screening) length may be metaphorized as the maximum distance a person can see in a forest

2.2.2 Radiation

The ever present hazard to life and machine alike, radiation is among the first factors to be considered when venturing to space. While living organisms may be able to cope with the damage in one way or another, protecting the rigid electronics can so far only be done by increasing their numbers (redundancy) and shielding. Exposed to radiation the electronic components will degrade, setting a hard limit for the lifetime of the scientific payload on a spacecraft. In case of the Cassini RPWS/LP, such degradation was not expected to occur before mission end (even if counting the time extensions) given the estimated radiation hazards. However, during the extended mission in 2008, the Cassini spacecraft found itself in Saturn's radiation belts during ~9 consecutive orbits and the effects were felt by the RPWS/LP as illustrated in **Figure 4**[13]. The likely reason is that the unshielded pre-amplifier experienced radiation degradation.

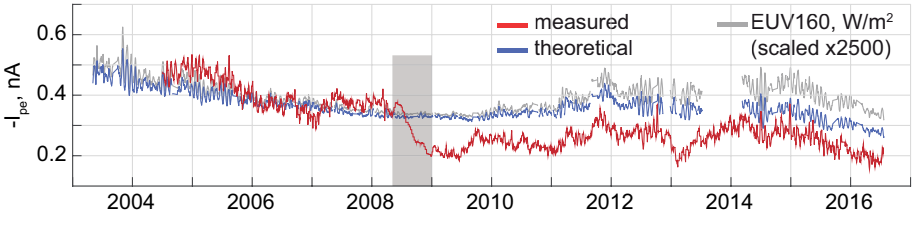

Figure 4. *Degradation of the RPWS/LP current due to radiation damage, shown on the example of the measured photoelectron current (**red**) versus the theoretical current (**blue**), derived using the TIMED/SEE and SORCE/ SOLSTICE measurements of solar EUV up to 160 nm translated to Saturn (grey). The period of high radiation is marked with the grey rectangle. Adapted from Paper III.*

This effect permeates all RPWS/LP measurements and is trivially removed like any systematic factor. Measuring the photoelectron current (I_{pe}) itself requires a correction which has been derived in Paper III.

2.3 Spacecraft-Plasma interactions

An object immersed in a plasma will be hit by the charge carriers, some giving it the charge and some taking it away. This means that an object in a plasma will accumulate potential (in relation to the plasma) until the net

[13] The EUV flux here is a combination of the measurements by the **T**hermosphere **I**onosphere **M**esosphere **E**nergetics and **D**ynamics (**TIMED**) **S**olar **E**UV **E**xperiment (**SEE**) and the **So**lar **R**adiation and **C**limate **E**xperiment (**SORCE**) **Sol**ar **St**ellar **I**rradiance **C**omparison **E**xperiment (**SOLSTICE**)

charge flux is zero; for the spacecraft applications it is of course called the spacecraft potential (U_{sc}). Additionally, particle impacts may produce secondary electron emission and a spacecraft in sunlight will be subject to the photoelectric effect. All of these factors add up to the net charge flux ($\sum I_{sc} = 0$) that determines the spacecraft potential. These and related issues are discussed below.

2.3.1 Spacecraft surface charging

Awareness of spacecraft charging began with the first ionosphere measurements with rockets. The charging of an object in plasma usually depends only on the electron energies, temperatures and densities, since the flux of electrons is typically much larger than the flux of much heavier ions. Furthermore, in a dense plasma (e.g., an ionosphere, $I_{ions}, I_e \gg I_{pe}$) the U_{sc} is only dependent on the electron temperature; in a tenuous plasma ($I_{ions} \ll I_e \sim I_{pe}$) it may be used to derive the charge densities [*Garrett and Whittlesey*, 2000]. In dusty plasmas (described below), the metallic parts of a spacecraft (and instruments) are subject to triboelectric charging: a charge transfer from dust particles due to frictional contact or a difference in work functions between the dust and metal surfaces [*Barjatya and Swenson*, 2006], a yet another mechanism that influences the spacecraft potential. However, the Cassini spacecraft has so far not detected any triboelectric effects in dust-rich environments like Enceladus' plume [*Morooka et al.*, 2011] and deep ionosphere of Titan [*Wahlund et al.*, 2009b].

Potential of the RPWS/LP on Cassini is defined relative to U_{sc} so the latter can be measured "directly". In Titan's ionosphere, the measured Cassini spacecraft potential is very stable between approximately -1.5 and -0.5 V [*Wahlund*, 2005; *Ågren et al.*, 2007]. The photoelectric effect adds 0.1 to 0.2 V on the dayside (compared to the nightside). Below ~ 1600 km altitude, the spacecraft surface charging does not affect the ion and electron measurements by the RPWS/LP beyond a trivial correction because the instrument is mounted on an 1.5 m boom – much longer than the local Debye length of $\lesssim 8$ cm[14]. Generally though, the spacecraft charging is of great concern for all missions and must be taken into account at design stage – depending on the environment, U_{sc} can reach kilovolts [*Eriksson and Wahlund*, 2006]. The common practice is to make a surface of the spacecraft conductive to equilibrate the potential and avoid the potential differences that cause arc discharges and fry the electronics.

[14] Instruments mounted closer than one Debye length may not measure the complete energy distribution of the plasma particles because the spacecraft potential acts as a barrier (as an example, $U_{sc} = -1$ V can only be passed by electrons with energies ≥ 1 eV, etc.)

2.3.2 Wake effects

A plasma wake forms in a supersonic flow behind the spacecraft, when the kinetic energy of plasma ions $m_i v_i^2/2$ exceeds their thermal energy $k_b T_i$ (and the spacecraft potential energy eU_{sc}). Electrons are most often subsonic in an ionosphere, which means that while ions are depleted in a wake, electrons fill it up, giving it a negative potential. If the $m_i v_i^2/2 < eU_{sc}$, the ions will not reach the spacecraft at all and an enhanced wake will form (**Figure 5**). For the Cassini spacecraft, **Figure 5a** shows a typical wake in Titan's ionosphere ($U_{sc} \sim -0.5$V, but the ion velocity is close to the spacecraft velocity, ≈ 6 kms^{-1}), whereas the enhanced wake (**Figure 5b**) is relevant for regions of tenuous plasma in Saturn's magnetosphere.

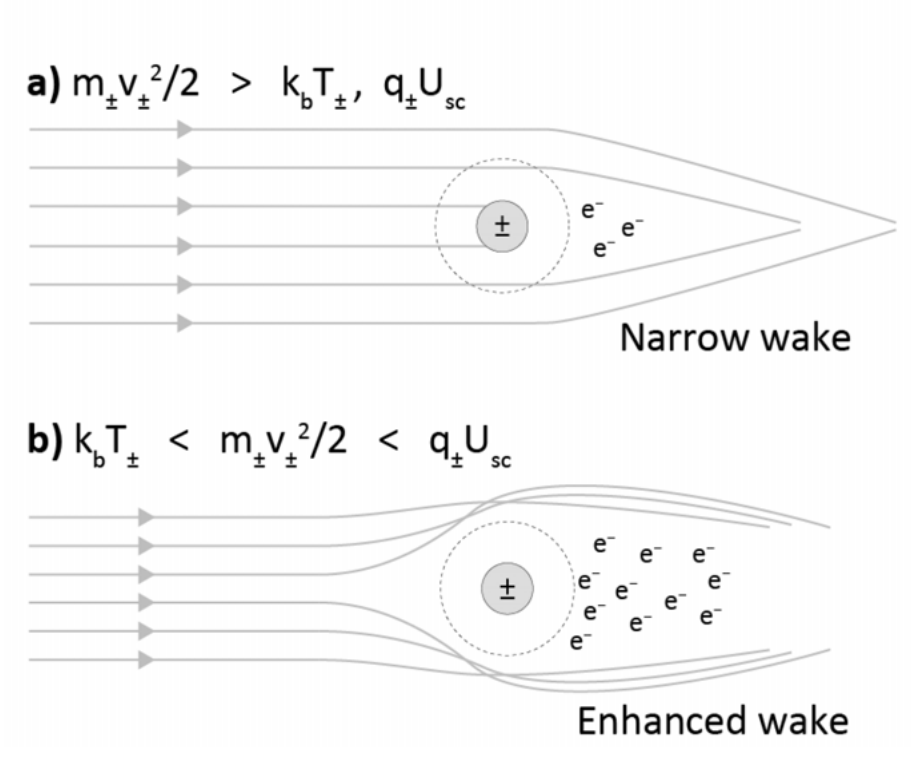

Figure 5. *Wake formation in a supersonic plasma. When the kinetic energy of the ions $mv^2/2$ is higher than the spacecraft potential energy (**a**), the wake is defined by the spacecraft geometry. In reverse case (**b**), the wake is defined by the equipotential surface that corresponds to the ion kinetic energy. Adapted from Eriksson et al., 2006.*

The spacecraft attitude may be adjusted to position the plasma measurement instruments outside the wake. Interestingly, although the wake artefacts are undesirable, some plasma properties can be derived from wake formation – for instance, a flow velocity vector can be estimated by applying

a model to combined measurements of two LP probes and an electron drift instrument [*Engwall et al.*, 2006].

During the RPWS/LP measurements of Titan's ionosphere, the probe measured the Cassini spacecraft wake during three early flybys, T3, T8 and T13. T3 and T8 are outside the altitude range relevant for this work, T13 data has been removed from the dataset.

2.4 Ion measurements: the clockworks

The datasets included in the works summarized here are primarily from the instruments onboard the Cassini spacecraft (**Figure 6**): the Radio and Plasma Wave Science (RPWS) Langmuir Probe (LP) and the particle instruments, the Ion and Neutral Mass Spectrometer (INMS), the Cassini Plasma Science (CAPS) Ion Beam Spectrometer (IBS) and Electron Spectrometer (ELS).

Additionally, solar EUV measurements by the Thermosphere Ionosphere Mesosphere Energetics and Dynamics (TIMED) Solar EUV Experiment (SEE)[15] and the Solar Radiation and Climate Experiment (SORCE) Solar Stellar Irradiance Comparison Experiment (SOLSTICE)[16] were used for the photoelectron current correction in Paper III and as input in the ionosphere model in Paper IV. This section gives a brief overview of the instruments onboard the Cassini spacecraft.

[15] http://lasp.colorado.edu/lisird/see/

[16] http://lasp.colorado.edu/lisird/sorce/

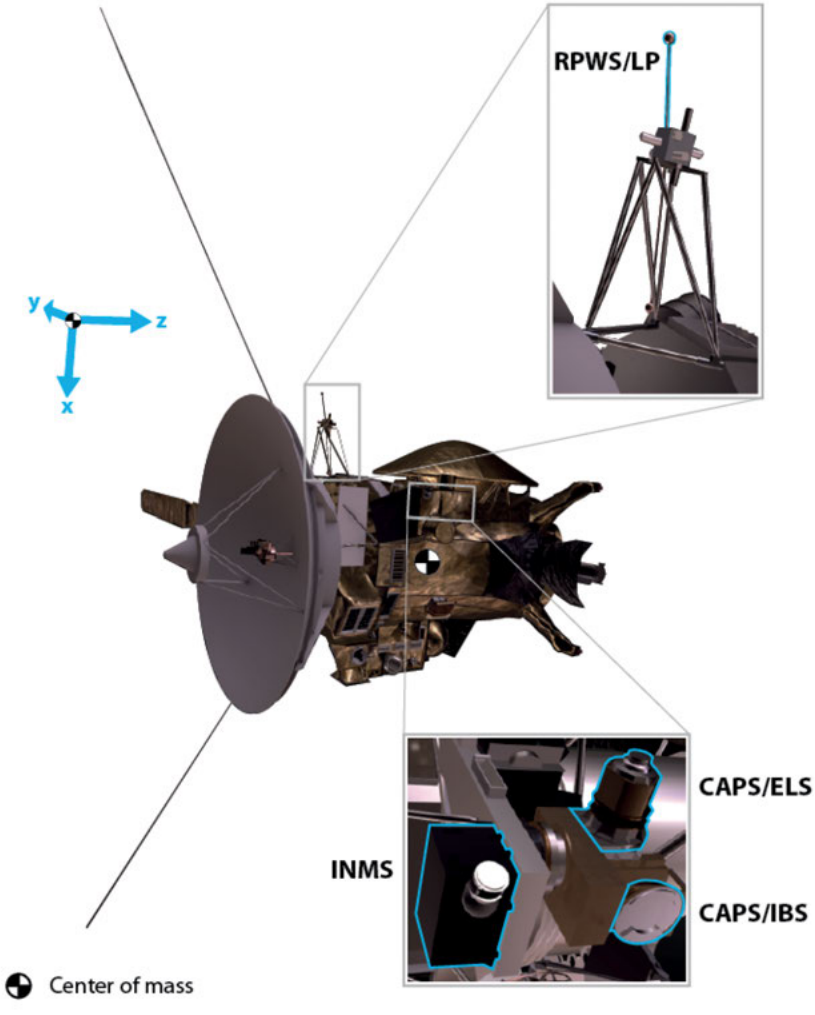

Figure 6. *3D model[17] of the Cassini-Huygens spacecraft, showing the locations of the RPWS/LP, INMS and CAPS instruments. The spacecraft coordinate system is shown in blue (y-axis is directed into the paper), with origin at the spacecraft center of mass.*

[17] Source: https://saturn.jpl.nasa.gov/the-journey/the-spacecraft/.

2.4.1 Langmuir probe (RPWS/LP)

Electrostatic probes, or more commonly, Langmuir probes, named after their inventor Irving Langmuir, $1881-1957$, have been used for measurements of ionized gas properties for almost a century, since their introduction in 1924[18] and theoretical description in 1926 [*Mott-Smith and Langmuir*, 1926]. The principles of LPs are trivial: collecting a current from a plasma by applying a bias voltage to the probe; by altering the voltage a current-voltage characteristic curve of the plasma is obtained. From this curve, various parameters of the plasma's electrons and ions may then be derived.

The Cassini RPWS/LP has been built and is operated by the Swedish Institute of Space Physics. It is a titanium sphere with radius of 2.5 cm (coated in TiN), mounted on a 1.24 m boom (**Figure 7**). Three modes of operation are used: voltage sweep, density and cleaning [*Gurnett et al.*, 2004].

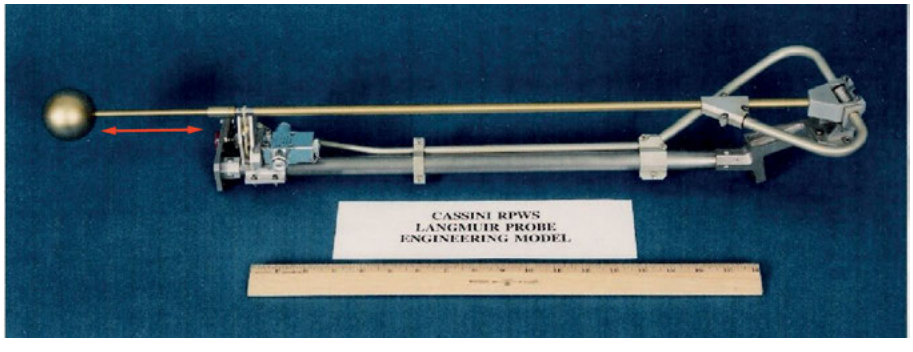

Figure 7. *Cassini RWPS/LP (radius* 2.5 *cm) and its deployment mechanism (engineering model). Total distance from the spacecraft when deployed is* 1.24 *m. The red arrow marks the stub that is kept at the same potential as the probe, to shield it from the spacecraft photo- and secondary electrons (this configuration also makes the LP potential distribution more spherical). Both the probe and the stub are made of titanium with TiN coating. Note that the reference ruler is in inches, not cm.*

Voltage sweeps measure the current to the probe for voltage ranges of ± 32 V or ± 4 V (for targeted flybys of moons) every 24 s shifting the voltage in 512 steps during 0.5 s. For Titan flybys, the speed of the Cassini spacecraft (v_{sc}) is ~ 6 kms^{-1}, limiting the spatial resolution of the RPWS/LP to ≈ 3 km). Targeted flybys usually have double-sweeps, from the positive bias voltage to the negative and then back to the positive, giving 1024 points. To monitor capacitive charging effects[19], the current is sampled twice, just after the

[18] I. Langmuir and H. Mott-Smith, General Electric Review, Vol. **27**, 449, 538, 616, 762, 810 (1924). Not digitized, no DOI available.

[19] Capacitors in the circuitry don't allow the current to instantly adapt to the voltage change

voltage shift and just before the next shift. Voltage sweep mode yields the current-voltage characteristic curve for deriving electron and ion parameters. The ion part of the sweep (negative bias voltage) is the primary dataset for the work included in this thesis.

The density mode sets the probe to a constant voltage, allowing high frequency (20 Hz) sampling of the current, used mostly for electron measurements. The cleaning mode is used on a regular basis to remove possible contamination of the probe surface. This is done by setting the probe to $+32$ V and sputtering the surface with high energy electrons.

2.4.1.1 Orbital-Motion Limited theory

Here we review the general probe theory for the ion measurements and the somewhat special case of Titan's ionosphere. In practice, every plasma has its own caveats and the analysis has to be tailored for it, but each application is derived from the common theory – the Orbital-Motion Limited theory, hereafter referred to as OML. It is based on independent trajectories of a particle speed distribution (Maxwellian for our purposes) to sort out the particles that are measured, i.e., that have trajectories ending on the probe surface. The trajectories are defined by conservations of energy and angular momentum (the latter is optional, as demonstrated by *Laframboise and Parker*, 1973).

The following conditions have to be met for the OML:

i) no particle originates from the probe, and
ii) the radius of the probe must be (much) smaller than one Debye length, λ_D.

For the probe dimensions comparable to λ_D the Sheath Limited theory should be used instead. The OML works fine for the Cassini RPWS/LP (radius 2.5 cm) in the ionospheric plasma of Titan where $\lambda_D \sim 3 - 8$ cm.

The original equations for laboratory isotropic plasma by *Mott-Smith and Langmuir*, 1926 were upgraded by *Medicus*, 1962 for a plasma in motion (drifting) relative to the probe, which is typical in space applications. Additionally, *Laframboise and Parker*, 1973 showed that the expression for ideal spheres also holds for some deviations from the perfect shape, such a spherical probe on a stub like the Cassini RPWS/LP (**Figure 7**). Generally, the collected current I for a probe of radius r_{lp} and bias potential U is[20]:

[20] Equation [1] is obtained by integrating the Maxwellian velocity distribution of the plasma particles that reach the probe, see e.g. *Whipple*, 1965; *Engwall*, 2006

$$I = -qnr_{lp}^2 \cdot \sqrt{\frac{\pi k_b T}{2m}} \cdot \left[e^{-A} \cdot \left(1 - \frac{v_1}{v_{sc}} \right) + e^{-B} \cdot \left(1 + \frac{v_1}{v_{sc}} \right) + \sqrt{\frac{\pi k_b T}{2mv_{sc}^2}} \cdot \left(\frac{mv_{sc}^2}{k_b T} + 1 - \frac{2qU}{k_b T} \right) \cdot \left(\mathrm{erf}\left(\sqrt{A}\right) - \mathrm{erf}\left(\sqrt{B}\right) \right) \right], \quad [1]$$

where q, n, m and T are particle (ion) charge, density, mass and temperature resp., k_b is the Boltzmann constant and v_{sc} is the spacecraft speed relative to the plasma (SI units), $A = m(2k_bT)^{-1}(v_1 + v_{sc})^2$, $B = m(2k_bT)^{-1}(v_1 - v_{sc})^2$, $\mathrm{erf}(x) = 2\pi^{-0.5} \int_0^x \exp(-y^2)\, dy$ (error function) and v_1 is the minimum relative speed a particle (ion) needs to overcome the potential barrier defines as $v_1 = \sqrt{2qU/m}$ for repelling potentials ($qU > 0$) and $v_1 = 0$ for attracting potentials ($qU < 0$).

2.4.1.2 Photoelectron current

An important effect to consider for Langmuir probe measurements in space is the photoelectron emission. Lab experiments by *Grard*, 1973 have shown that although photoelectron current (I_{pe}) depends on the material, the energy distribution shape is similar to (and can be approximated by) a double-Maxwellian with a dominant peak at ~ 2 eV. If the photoelectron sheaths of the probe and spacecraft overlap a "stray" current may leak through. The Cassini RPWS/LP is mounted on a stub (**Figure 7**) and the probe often shadows the stub (in addition to the spacecraft shadowing), so that I_{pe} depends on the spacecraft attitude [*Jacobsen et al.*, 2009; *Morooka et al.*, 2009; *Holmberg et al.*, 2012]. For Titan's ionosphere, I_{pe} is typically negligible, being an order of magnitude smaller than the ion current at altitudes of $1600 - 1400$ km and vanishing completely due to solar EUV extinction below ~1400 km altitudes. Regardless, it is removed in the analysis as a standard procedure, see *Ågren et al.*, 2007 and Paper III for details.

2.4.1.3 Ion current

The ion current in Titan's ionosphere has been observed to be linear (within the instrument noise level of 100 pA) for the bias voltage range of $\pm$4V, proving eq. [1] to be unnecessarily complicated. Instead, an approximation by *Fahleson et al.*, 1974 is employed, giving current for *one ion species* as

$$I \approx \begin{cases} I_0(1-\chi) & \text{for } qU_{bias} < 0 \text{ (attracting potential)} \\ I_0 e^{-\chi} & \text{for } qU_{bias} > 0 \text{ (repelling potential)} \end{cases}, \quad [2]$$

where

$$I_0 \approx -qn\pi r_{lp}^2 \sqrt{\frac{v^2}{16} + \frac{k_b T}{2\pi m}} \text{ and } \approx \frac{2q|U_{bias} + U_{float}|}{mv^2 + 2k_b T} = \frac{2q|U|}{mv^2 + 2k_b T}, \quad [3]$$

U_{bias} is the probe potential and U_{float} is the spacecraft floating potential[21], determined by the spacecraft charging. These equations give an extremely good approximation for ion and electron currents compared to the full *Medicus*, 1962 expressions and are far easier to fit to data than eq. [1]. For ions, the thermal energy component k_bT can often be neglected[22] (since they are heavy) in a fast flowing plasma (i.e., a fast flying spacecraft). Furthermore, as mentioned above, the measured ion current is linear within the instrument noise level and for the negative ions χ is small due to their large mass and the $e^{-\chi}$ in eq. [2] can be approximated by $1-\chi$ [Paper I, II]. Assuming stationary ions (ion drifts are < 260 ms^{-1}, *Müller-Wodarg et al.*, 2008; *Crary et al.*, 2009), the spacecraft velocity is substituted as the ion velocity and the total ion current (summed over all the ion species i) is simplified into

$$I_{tot} \approx \overbrace{-\pi r_{lp}^2 \frac{|v_{sc}|}{4}\sum_i q_i n_i}^{DC\ current} + \overbrace{\frac{\pi r_{lp}^2}{2|v_{sc}|}\sum_i \frac{q_i^2 n_i}{m_i}}^{gradient}|U|. \qquad [4]$$

However, an LP cannot discriminate between different ion species (i.e., masses) since the total ion flux is collected – although the measurement is sensitive to ion mass. For the case of Titan's ionosphere, the problem becomes undetermined: the masses of negative and positive ions are necessary to derive the ion charge densities. The catch is that the masses do not add linearly but as a geometric sum, $\sum_i q_i^2 n_i m_i^{-1}$. The mass spectra may be obtained from the INMS, CAPS/IBS and CAPS/ELS instruments on the Cassini spacecraft [e.g., *Coates et al.*, 2009; *Crary et al.*, 2009; *Mandt et al.*, 2012]. Unfortunately, measurements of the said mass distributions are not available for every Titan flyby as the CAPS instruments were shut down in June 4th 2012[23]. The INMS data is available for a greater number of flybys but only for the lighter ions (capped at 99 amu). A solution was found in form an effective ion mass [Paper II], defined as

$$\frac{1}{m_{eff}} = \sum_i \frac{z_i n_i'}{m_i/z_i}. \qquad [5]$$

Here z_i is the positive (negative) ion charge number, m_i/z_i is the positive (negative) ion mass/charge measured by the CAPS/IBS (CAPS/ELS) and n_i', and the relative abundance of positive (negative) ion species i, normalized to the total positive (negative) charge density. The effective mass is derived as

---

[21] Defined for a certain *surface* on a spacecraft, not to be confused with the spacecraft potential

[22] This introduces errors of $< 0.1\%$ in Titan's ionosphere below 1400 km altitudes (~150 K, 28 amu ions with spacecraft-relative velocities ~6 kms^{-1}), well below the RPWS/LP instrument error

[23] http://saturn.jpl.nasa.gov/news/significantevents/anomalies/

an empirical function of the INMS mean ion mass (of the ≤ 99 amu ions) using the INMS, CAPS/IBS and CAPS/ELS data from select Titan flybys. This is possible because the heavier ions originate from the lighter ions (for details on this method see Paper II). The derived effective ion mass is applicable to all Titan flybys and may be improved with the updated CAPS/ELS analysis of the negative ions.

Substituting eq. [5] into eq. [4], assuming quasi-neutrality, singly-charged positive ions [*Thissen et al.*, 2011] and adding the positive and negative ion currents, the final expression for the total ion current is obtained:

$$I_{tot} \approx \overbrace{q_e \pi r_{lp}^2 |v_{sc}| (z\_n\_ - n_+)}^{DC-current} + \overbrace{\frac{2q_e \pi r_{lp}^2}{|v_{sc}|}\left(\frac{z\_n\_}{m_{eff-}} + \frac{n_+}{m_{eff+}}\right)}^{gradient} |U|, \qquad [6]$$

where n_+ and $z\_n\_$ are the total positive and negative charge densities, respectively and q_e is the elementary (electron) charge. Derivation of the ion charge densities from the sweep data is performed as follows. The double-sampled[24] current values are averaged, the photoelectron current is removed and the remaining total measured ion current is fitted to $m = a - |U| \cdot b$ by a least squares linear regression (see example in **Figure 8**), yielding the gradient b and the DC current a (compare with eq. [4]). Fits with residuals exceeding the noise level of 100 pA are flagged for investigation. Due to the "simplicity" of the ion current theory the process can be largely automated.

Positive and negative ion charge densities may be derived from the obtained fit parameters a and b by identification with eq. [6]:

$$\begin{cases} q_e \pi r_{lp}^2 |v_{sc}| (z\_n\_ - n_+) = a \\ \frac{2q_e \pi r_{lp}^2}{|v_{sc}|}\left(\frac{z\_n\_}{m_{eff-}} + \frac{n_+}{m_{eff+}}\right) = -b \end{cases}, \qquad [7]$$

or, with the known quantities grouped together

$$\begin{cases} z\_n\_ - n_+ = \frac{a}{q_e \pi r_{lp}^2 |v_{sc}|} = A \\ \frac{z\_n\_}{m_{eff-}} + \frac{n_+}{m_{eff+}} = \frac{-b|v_{sc}|}{2q_e \pi r_{lp}^2} = B \end{cases}. \qquad [8]$$

Solving for the charge densities, we obtain[25]

[24] before and after a voltage shift

[25] same as eq. 6-8 in Paper II, with $m_{eff-}/Z\_$ replaced by m_{eff-} and r_{lp} by r_{lp}^2 (typos).

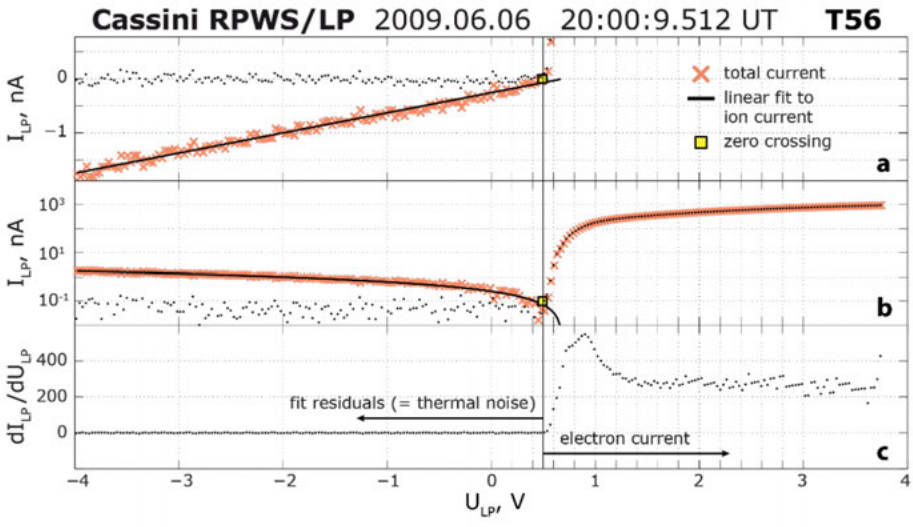

Figure 8. *Ion current fit example from Titan's ionosphere, flyby T56. The* ***total sampled current*** *and a* ***linear fit*** *to the ion current is plotted on a linear scale (**a**, vertically zoomed on the ion current) and a log scale for comparison with the electron current (**b**). The* ***black dots*** *are fit residuals, representing the thermal noise for the negative potentials (relative plasma) and the electron current for the positive potentials (where the fit is zero).*

$$\begin{cases} n_+ = \left(Bm_{eff-} - A\right)\left(\frac{m_{eff-}}{m_{eff+}} + 1\right)^{-1} \\ z_- n_- = \left(Bm_{eff+} + A\right)\left(\frac{m_{eff+}}{m_{eff-}} + 1\right)^{-1} \end{cases}. \qquad [9]$$

The uncertainties in the fit parameters a and b are given by $2\sigma_a \sim 10^{-12}$ cm^{-3} and $2\sigma_b \sim 10^{-8}$ cm^{-3}. The effective mass has an uncertainty from the empirical fit, corresponding to $2\sigma_{meff\pm} \sim 100$ cm^{-3}. Additionally, the CAPS/ELS derived negative ion mass/charge (relevant for m_{eff-}) has uncertainties of $\leq 50\%$ [*Wellbrock et al.*, 2013]. All these propagate to total uncertainties of the charge densities, $2\sigma_\pm \leq 400$ cm^{-3} or $\leq 20\%$ of the measured peak/maximum values. It should be noted that throughout this work we use electron densities derived from the ion part of the sweep the equation [8] as $n_e = -A$, due to the possible negative ion contamination of the electron current (positive bias voltage part of the sweep). Some examples of this are shown in **Figure 9**.

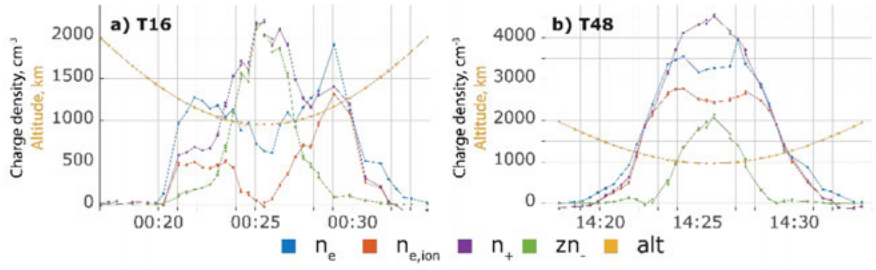

Figure 9. *Examples of the negative ion contamination of the electron densities derived from the electron currents from flybys T16 (**a**), T48 (**b**). The electron density derived from the electron current (blue) is larger than the electron density derived from the ion current (red) in regions with the negative ions (green), and even larger than the positive ion densities (purple) during T16 (**a**). Altitude is shown in yellow for reference. Adapted from Paper IV.*

2.4.2 Ion and Neutral Mass Spectrometer (INMS)

The INMS was designed and manufactured at NASA's Goddard Space Flight Centre's Planetary Atmospheres Laboratory and the University of Michigan's Space Physics Research Laboratory. It is a high-resolution (1 amu) particle spectrometer for measuring the mass distribution of ions and neutral gas up to 99 amu [*Mandt et al.*, 2012] with two modes of operation, closed ion source and open ion source (see **Figure 10**).

In closed ion source (**Figure 10a**), the neutral gas is ping-ponged on the walls of the spherical antechamber, reaching thermal equilibrium. The antechamber geometry creates a pressure gradient that drives the gas to the ion source, where it is ionized by the electron guns G1 & G2 and focused into the quadrupole mass analyser (**Figure 10e**) by the quadrupole and electrostatic switching lenses (**Figure 10c**, **d**).

In open ion source (**Figure 10b**), the ions (or neutrals, ionized by the electron guns G1 & G2) are directed into the same path by the quadrupole switching lens (**Figure 10c**). When measuring the neutrals, the ions get trapped by the deflectors in the cylindrical part of the antechamber. When measuring the ions the neutrals are not ionized and so not redirected by the quadrupole switching lens. In both cases, the particles are fed through the quadrupole mass analyser (**Figure 10e**), which separates them by mass-to-charge ratios, and sampled by the detector (**Figure 10f**). For the work presented in this thesis, the mean ion mass measurements (open ion source mode) were used.

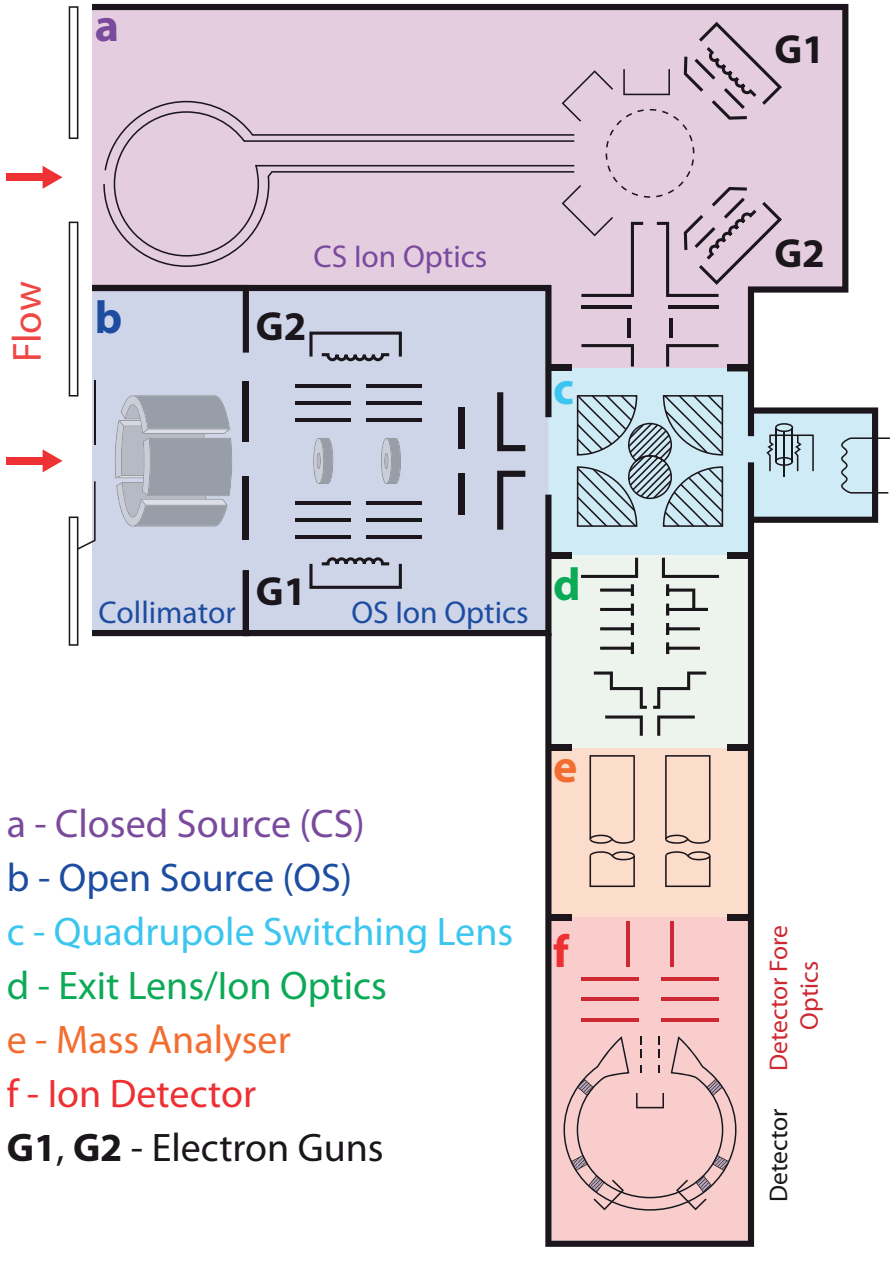

Figure 10. *Schematic representation of INMS (adapted from Mandt et al., 2012).*

2.4.3 Electron Spectrometer (CAPS/ELS)

Part of the Cassini Plasma Science package, the ELS (**Figure 11**) was designed and manufactured by the Mullard Space Science Laboratory (MSSL). The ELS is a hemispherical top-hat electrostatic analyser and both angular and energy resolutions are limited by its geometry and the micro-channel plate (8 anodes covering 20° each). During a measurement, ELS performs a sweep over log-spaced voltages in accumulation intervals of 31.25 ms (for Titan, the default mode is 64 steps covering $0.6 - 28000$ eV). As an electrostatic analyser, the raw output of the ELS is *energy/charge*, from which the mass/charge and density/charge are then derived. This is especially relevant for the negative ion measurements as they may have multiple charges. Fact is that the instrument was not intended for measuring the negative ions at

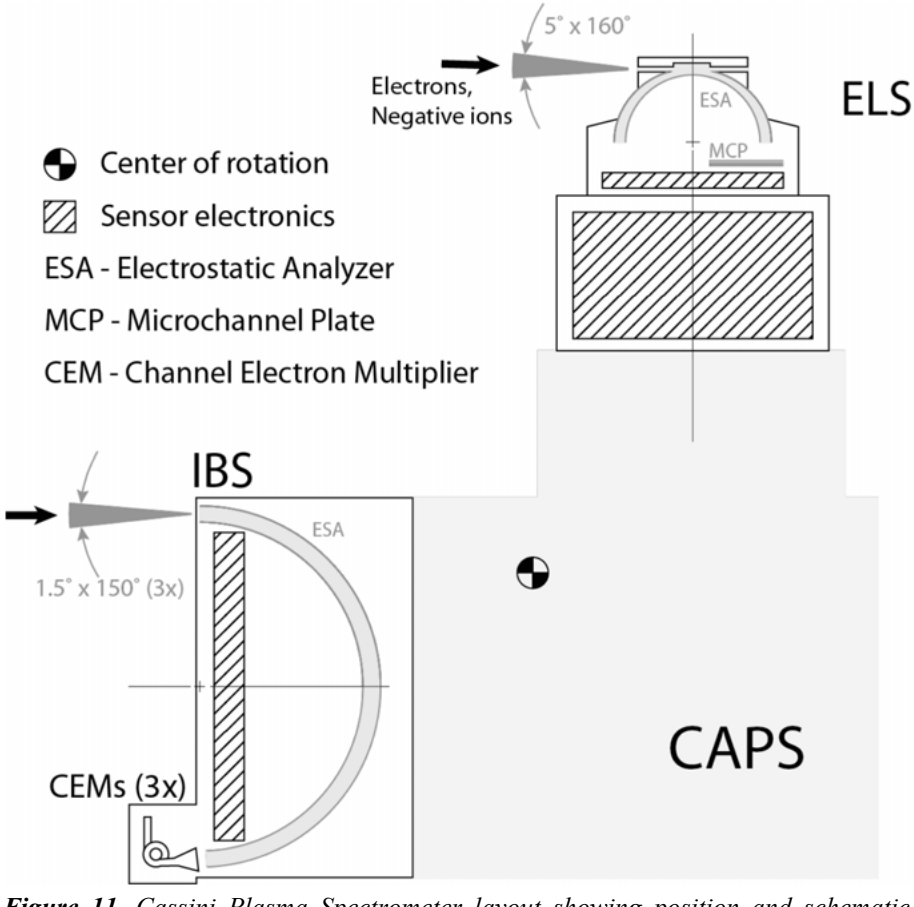

Figure 11. *Cassini Plasma Spectrometer layout showing position and schematic representation of the IBS and ELS instruments. IBS has three apertures (symbolized with 3x), each with its own channel electron multiplier (CEM) detector, allowing determination of a 3D plasma velocity distribution. Adapted from Young et al., 2004.*

all and their detection [*Coates et al.*, 2007, 2009] is a serendipitous boon despite the rather conservative density/charge uncertainty upper limit of 50% [*Wellbrock et al.*, 2013]. An example of the ELS negative ion mass spectrum is shown in **Figure 12b**.

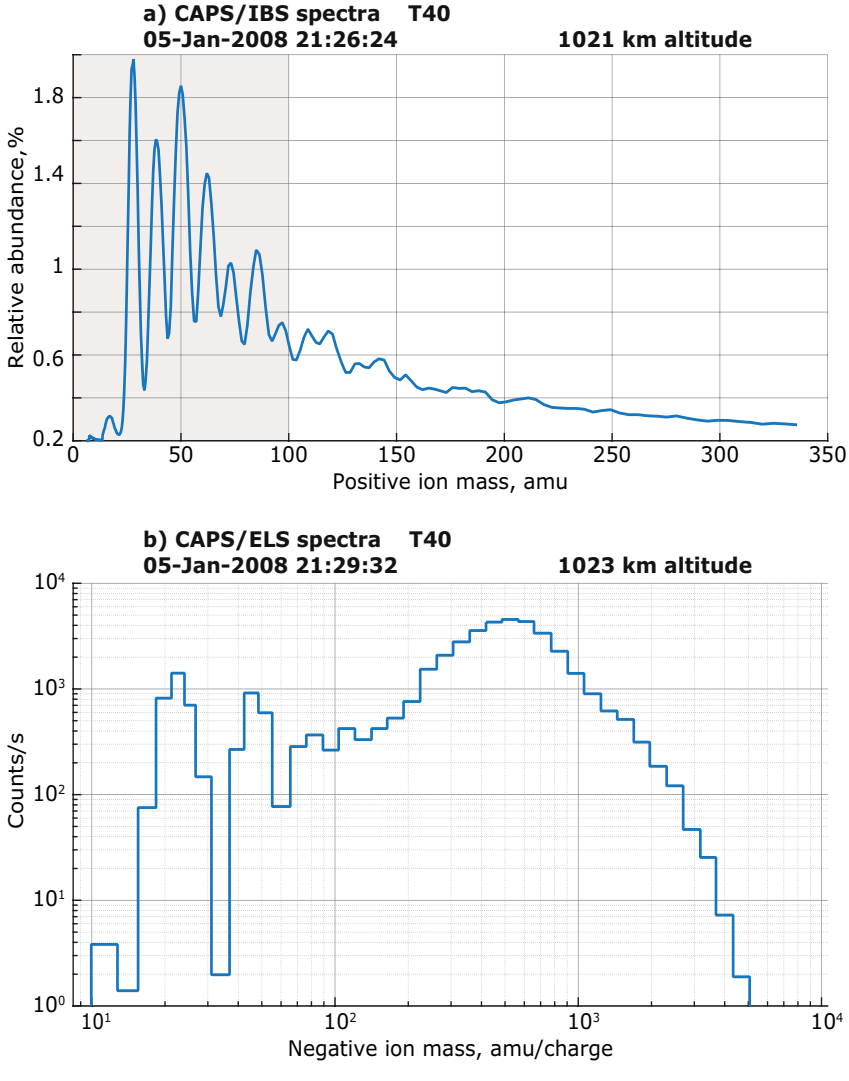

Figure 12. *Mass spectra examples from the T40 flyby at altitude ≈ 1020 km:* ***a)*** *CAPS/IBS, shaded area shows the part seen also by the INMS;* ***b)*** *CAPS/ELS, the wide peak at ~400 amu/q corresponds to the dust grain (aerosol) precursors. Adapted from Paper II.*

2.4.4 Ion Beam Spectrometer (CAPS/IBS)

The Ion Beam Spectrometer (IBS) is a curved-electrode electrostatic analyser (**Figure 11**), designed and manufactured by the Southwest Research Institute (SWRI) to provide high-resolution measurements of the positive ion flux over $0.6 - 28250$ eV energy range. During operation the IBS performs a voltage scan in 255 steps over 2 s, its architecture allows it to provide 80% coverage of all space [*Young et al.*, 2004]. Translating the energy range to mass (energy/charge and mass/charge actually, but the positive ions are unlikely to have > 1 charge, *Thissen et al.*, 2011), the IBS may provide the positive ion mass distribution up to ~ 1500 amu, covering the vast majority of the positive ion species in Titan's ionosphere as the larger particles tend to be negatively charged. However, the mass (i.e., energy) resolution of the IBS does not allow it to distinguish ions with similar masses in Titan's ionosphere [*Crary et al.*, 2009]. An example of the IBS positive ion mass spectrum is shown in **Figure 12a**.

3 Titan's Ionosphere

If you try and take a cat apart to see how it works, the first thing you have on your hands is a non-working cat.

— Douglas Adams

The ionosphere of Titan is conductive [*Rosenqvist et al.*, 2009; *Ågren et al.*, 2011] and takes credit for Titan's induced magnetosphere: the interaction between the ionosphere and Saturn's magnetic field (and its plasma) drapes Saturn's magnetic field lines around Titan, effectively creating a magnetosphere complete with an elongated tail around the moon . This interaction also contributes to exospheric escape of neutrals by charge exchange collisions [*Johnson et al.*, 2010; *Strobel and Cui*, 2014, and references therein] and ion escape [*Edberg et al.*, 2011]. Titan's ionosphere in Saturn's magnetospheric plasma thus resembles the ionospheres of Mars and Venus in the solar wind [*Nagy et al.*, 2004], with two differences: the direction of the incoming magnetospheric plasma flow is not always aligned with the Sun-ward direction for Titan, and the Kronian magnetospheric plasma is sub-magnetosonic, meaning that no bow shock is formed at Titan [e.g., *Wahlund et al.*, 2014 and references therein]. The accumulated knowledge of Titan's ionosphere should also be of some relevance for the future studies of Ganymede's ionosphere by the JUICE[26] mission (launch planned in 2022), as both moons are situated in the sub-magnetosonic magnetospheric plasma of their parent planets (although Ganymede has its own magnetic field).

3.1 Origin

The *in-situ* measurements by the Cassini spacecraft revealed the atmosphere of Titan to be primarily ionized by the solar EUV on the dayside and by energetic particles from Saturn's magnetosphere on the nightside, between ~800 and 1400 km altitude (**Figure 13**, **Figure 14**, see also *Ågren et al.*, 2007, 2009; *Cravens et al.*, 2008; Paper I, II). For the nightside, contributions from the dayside remnants are also possible [*Cui et al.*, 2009; Paper III]. Remote sensing of the ionosphere by the Cassini instruments in the $400 - 900$ km altitude range also showed minor ionization by the more energetic sources: magnetospheric ions, $\gtrsim 10$ keV electrons, micrometeoroids, solar hard X-ray and MeV proton events. The Huygens

[26] **Ju**piter **Ic**y Moons **E**xplorer, http://sci.esa.int/juice/

probe detected an ionosphere as low as at altitudes of $90 - 100$ km (matching modelled location of the ionization by the galactic cosmic rays) with plasma densities comparable to those produced by the solar EUV ionization at 1300 km altitude [e.g., *Galand et al.*, 2014, and references therein]. This thesis is based on the *in-situ* measurements by the Cassini spacecraft, setting the altitude region of interest to $880 - 1600$ km.

3.1.1 Solar EUV ionization

Since the main ionization source for Titan's dayside ionosphere is the solar EUV, the plasma densities vary significantly with the solar illumination. The latter depends on the column density of the neutrals, following the classical Chapman theory above ~1200 km altitude [*Edberg et al.*, 2013] and yielding a trend in altitude and solar zenith angle (SZA)[27] (**Figure 14**). The variation of the solar EUV flux across the solar cycle also influences Titan's ionosphere, the higher flux enhancing the densities of the primary species [*Madanian et al.*, 2016]; the overall ionospheric peak densities during the solar maximum conditions were found to be a factor ~2 higher than during the solar minimum [*Edberg et al.*, 2013; Paper III].

3.1.2 Particle impact ionization

The nightside ionosphere is primarily ionized by the impacts of energetic particles from the Kronian magnetosphere [*Ågren et al.*, 2007; *Cravens et al.*, 2009]. Possible transport of ions from the dayside has been highlighted [*Cui et al.*, 2009, 2010]. The particle ionization also occurs on the dayside, but is dwarfed by the solar EUV ionization down to ~1000 km altitude and becomes important well below the Cassini spacecraft flight altitudes as mentioned above. For the bulk ionosphere of Titan, the electron densities have been found to respond to Saturn's corotational plasma flow and Titan's position in Saturn's magnetosphere [*Edberg et al.*, 2015]. Isolating similar effects on the ion charge densities proved so far to be impossible with the RPWS/LP dataset [Paper III].

[27] Angle between the direction to the Sun and the position vector in a coordinate system, the angle is used to distinguish between the day, night and the region in-between called the terminator

3.2 Deep ionosphere

Typical altitude profiles of positive ions and negative ions/dust grains in Titan's ionosphere are shown in **Figure 13**. The biggest peaks from the *in-situ* observations are from the primary ionization sources as discussed above, but the maximum measured charge densities at the closest approach (~950 km altitude) often surpass the peak values by a factor of $\sim 1.5 - 2$, and a still larger peak is predicted (but not measured) for the dusty plasma layer below ~900 km altitude [Paper II]. Following the altitude trends, the second biggest variation in the charge densities is with the solar zenith angle (**Figure 14**). Due to the extent of Titan's atmosphere there is no sharp cut-off at the terminator, which stretches from 70° to 110° SZA [*Ågren et al.*, 2009; Paper I]. The EUV-induced ionosphere is fading along the ray path, which at the terminator translates to increasing altitudes of the corresponding ionospheric peaks (black lines in **Figure 14**, see also Figure 7 in *Ågren et al.*, 2009).

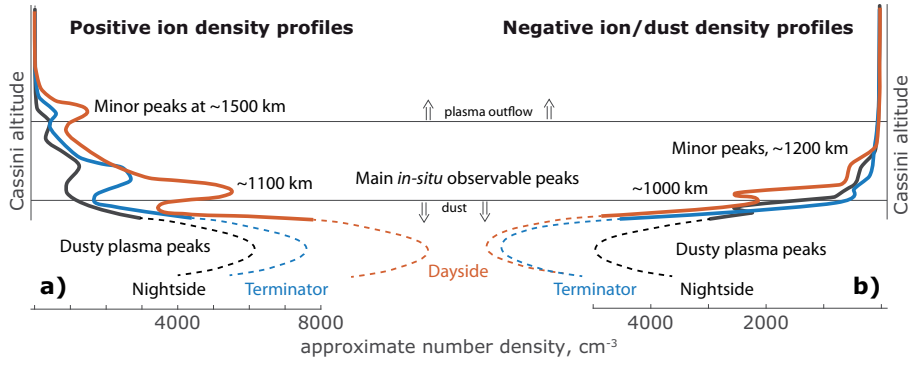

Figure 13. *A cartoon of* ***day****,* ***terminator*** *and* ***night*** *altitude profiles of the positive ions (**a**), and the negative ions and dust grains (**b**) in Titan's ionosphere (based on average charge density measurements by the RPWS/LP). The projected dusty plasma peaks are below the altitudes reachable by the Cassini spacecraft. Adapted from Paper III.*

Characteristic plasma densities can be inferred from **Figure 13** and **Figure 14** and are among the results of Paper I and II. **Figure 14** shows the charge density profiles of electrons (**a**), positive ions (**b**) and negative ions and dust grains (**c**), mapped to altitude and SZA (left side of the plots corresponds to the day ionosphere and right side – to the night. The map can be used to produce the altitude profiles for specific SZA, as shown in **Figure 15**. Divided by the SZA, Titan's ionosphere can be described by three parts:

SZA < 70°

Dayside, the ionosphere here is dominated by the positive ions and electrons ($\sim 3000 - 6000$ cm^{-3}) down to ~900 km altitude, where the electrons diminish and the negative ions ($\sim 2000 - 4000$ cm^{-3}) take over as the dominant negative charge carriers.

SZA 70°– 110°

Terminator, the overall charge densities ($\sim 2000 - 4000$ cm^{-3}) in this region gradually decrease while the peaks of the positive ion and electron densities appear at higher altitudes compared to the dayside; the negative ions become dominant negative charge carriers below 1100 km altitude.

SZA > 110°

Nightside, the electron densities are $\lesssim 500$ cm-3, the ionosphere at altitudes < 1100 km is dominated by the positive and negative ions ($\sim 2000 - 3000$ cm-3).

For all regions, we distinguish four components in Titan's ionospheric plasma: **1)** free electrons, **2)** positive ions, **3)** negative ions (up to macromolecules and clusters, < 1000 amu) and **4)** dust grains or aerosols (> 1000 amu, > 1 nm-sized). As the free electrons condense on the macromolecules and dust grains, the plasma becomes dusty, populated primarily by the ions (discussed in detail in section 0). Regarding variations of the solar illumination, there are two cycles at work, the solar cycle (≈ 11 years) and the orbital phase of Saturn (≈ 29.5 years). The latter is relevant due to the eccentricity of Saturn's orbit: the ionizing flux at aphelion (≈ 10 AU, northern hemisphere summer) is $\approx 23\%$ weaker than at perihelion (≈ 9 AU, northern hemisphere winter). The beginning of the Cassini mission (2004) saw northern hemisphere spring on Titan, with equinox in 2009. In the last two years of the mission ($2016 - 2017$), the northern hemisphere of the moon has had summer, which also coincided with solar maximum. By the end of mission, 15^{th} September 2017, the Cassini spacecraft has explored Saturn's system for almost half of a Kronian year ($\equiv$ Titan year[28]), making it possible to study seasonal changes of Titan's ionosphere in addition to the solar cycle.

The variation of Titan's dayside ionosphere with the solar EUV have been observed (by RPWS/LP and INMS) in the electron and ion charge densities, which were enhanced by a factor ~ 2 during the solar maximum, compared to minimum [*Edberg et al.*, 2013; *Madanian et al.*, 2016; Paper III] (see **Figure 16** and **Figure 17**). Remarkably, the EUV dependency of the dayside ion densities does not follow the Chapman theory below at least 1200 km, with the power law exponent deviating from the theoretical value of 0.5 by at least 2σ [Paper III]. The inapplicability of the Chapman theory in this altitude region is not too surprising: the theory assumes isothermality, plane-stratification, a single ion species and a flux of a single wavelength, none of which is valid at Titan – especially not below 1200 km altitude. The factor

[28] With a precision of ± 8 days, depending on Titan's position around Saturn

$\sim$2 enhancement of the dayside ion densities in **Figure 16** and **Figure 17** corresponds to $\sim$4000 cm^{-3} difference. The RPWS/LP measurements also suggest that the electron densities are $\approx$ 50% larger in summer compared to winter [*Edberg et al.*, 2013]. Investigation of the seasonal dependence of ions is unfortunately not possible with the RPWS/LP dataset as the SZA and EUV dependencies – the latter being a power law – must be removed first, which propagates errors too large to fit any further variables. For that reason the ion seasons, as well as the ionizing flux intensity variation between Saturn's perihelion and aphelion, remain an open question as a proper investigation would require at least 30 years of data and will hopefully be possible with the future missions to Titan.

Interestingly, the *nightside* of Titan's ionosphere is *not* oblivious to the solar cycle – measurements of the ion charge densities by the RPWS/LP reveal an anti-correlation with the solar EUV irradiance, the former diminishing by a factor $\sim 3-4$ from the solar minimum to maximum (corresponding to a difference of $\sim 3000-4000$ cm^{-3}) at altitudes < 1200 km [Paper III]. At these altitudes, the electrons are superseded by the negative ions [*Ågren et al.*, 2012; Paper I, II] and the ion-ion mutual neutralization gradually replaces ion-electron recombination as the main mechanism removing positive ions on the nightside [*Vigren et al.*, 2015]. In an ion-ion plasma with densities of $\sim$1000 cm^{-3} the average ion lifetime is estimated to $\sim$2 h. Even if such long-lived ions were formed on the dayside, they would not make it far into the nightside as the horizontal ion winds were estimated to be $\lesssim$ 260 ms^{-1} [*Müller-Wodarg et al.*, 2008; *Crary et al.*, 2009], making the transport timescale (at 1000 km altitude) $\gtrsim$ 13.5 h. In short, with ion lifetimes on the order of a few hours there should be no correlation between the EUV flux and the nightside ion densities (**Figure 18a**) as the ions there would be produced locally by the particle impacts. If on the other hand the transport was faster than the ion-ion reactions (i.e., ions were long-lived enough to last into the night), which also shares the effect with a super-rotating ionosphere, the correlation with the EUV flux would be the same as on the dayside – positive (**Figure 18b**). A mix of both long- and short-lived ions would also give a positive (albeit weaker) correlation (**Figure 18c**). Yet, none of these scenarios agree with the observations, represented schematically in **Figure 18d**. A speculative explanation, as suggested in Paper III, may be that the solar EUV changes the photochemistry of the dayside ionosphere by, e.g., enhancing the electron densities and the frequency of the photo-dissociation. The former boosts the rates of the dissociative recombination reactions that may terminate the reaction chains producing heavy complex organic molecules (HCOMs), while the latter eradicates those that have already formed. This would translate into more HCOMs surviving into the night at a lower solar EUV flux, and vice versa, fitting the observations (**Figure 18d**). Consequently, with less HCOMs on the nightside the electrons would have less attachment sites and deteriorate the positive ion densities by an increased electron recombination.

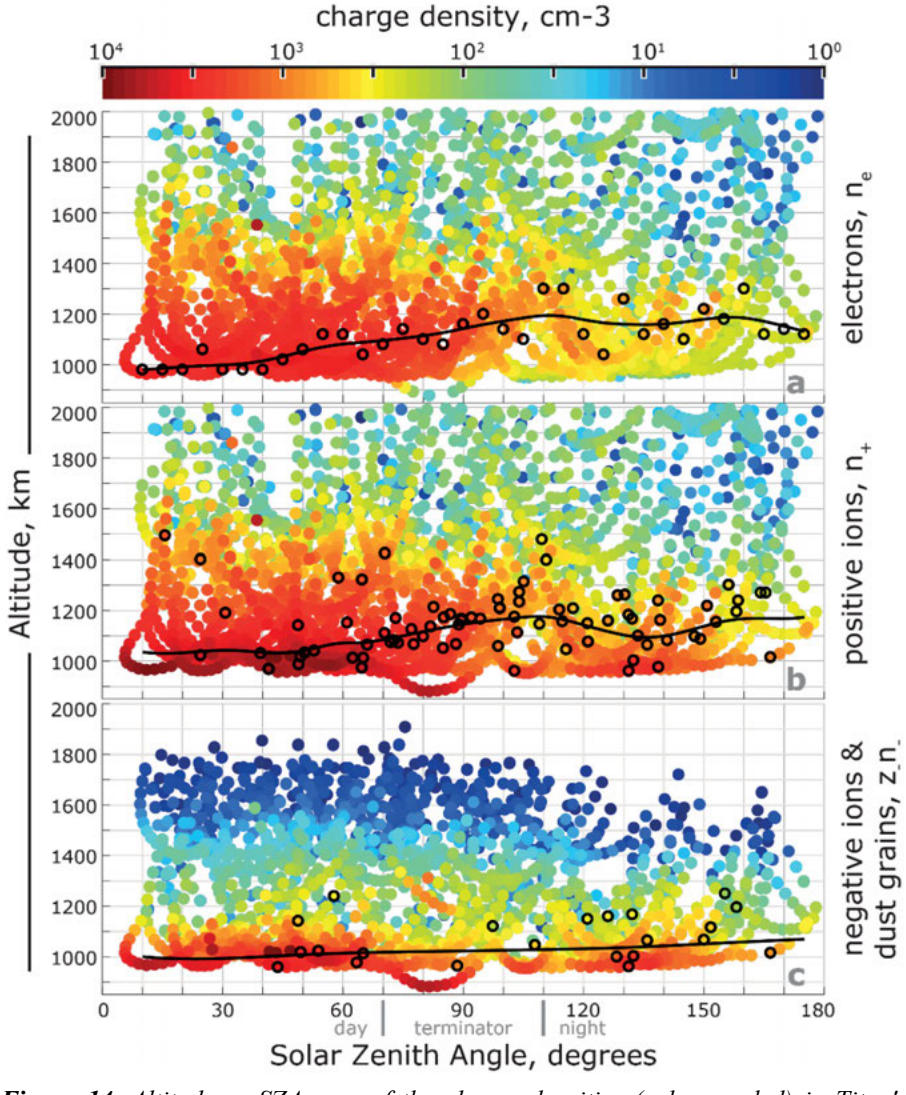

Figure 14. *Altitude vs SZA map of the charge densities (colour-coded) in Titan's ionosphere: electrons (**a**), positive ions (**b**), negative ions and dust grains (**c**).* ***Black lines*** *mark average altitudes of the primary charge densities peaks. Adapted from Paper I, updated with the latest flybys (TA-T120) and the analysis from Paper II.*

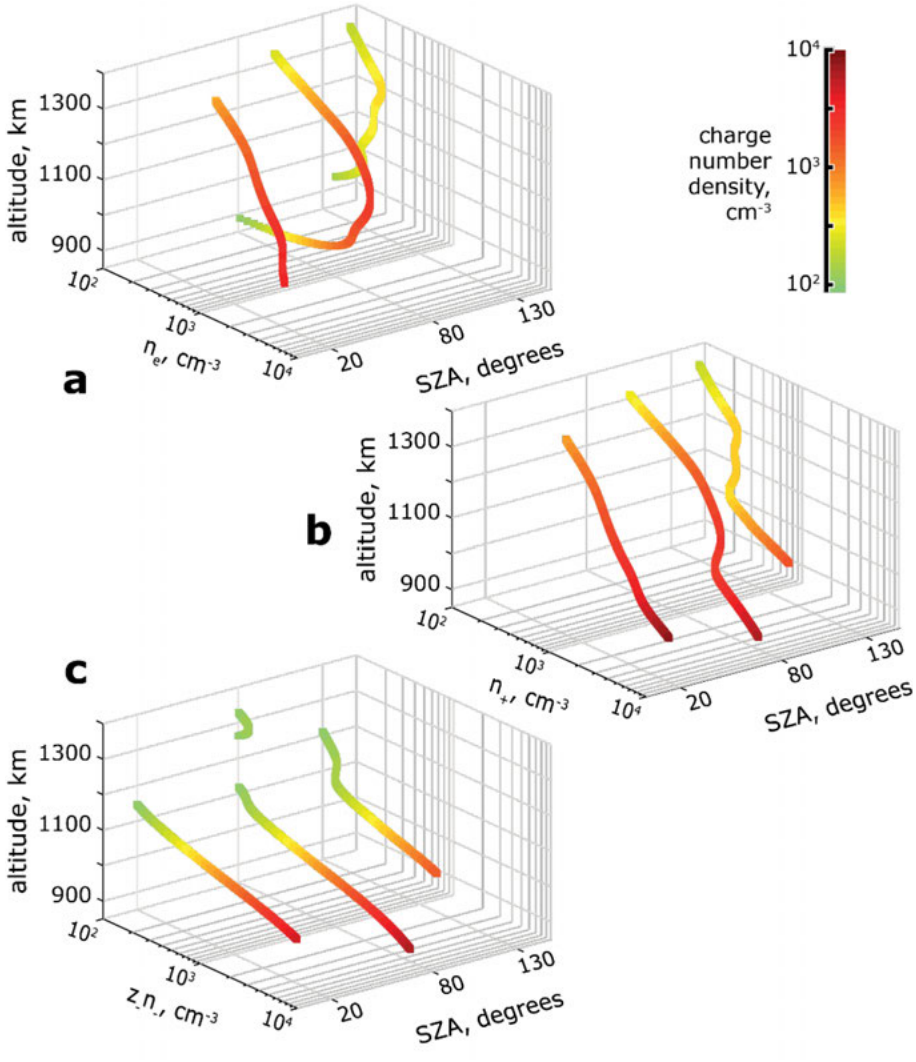

Figure 15. *Examples of the average ionospheric plasma density profiles in altitude, to clarify the ionosphere map in* ***Figure 14****. The profiles represent "slices" of the corresponding plasma charge densities at* 20°, 80° *and* 130° *SZA, interpolated in SZA bins* 15° – 20° *(dayside example),* 75° – 80° *(terminator example) and* 125° – 130° *(nightside example), respectively. The colour scale is the same as in* ***Figure 14*** *(but note the different altitude range).*

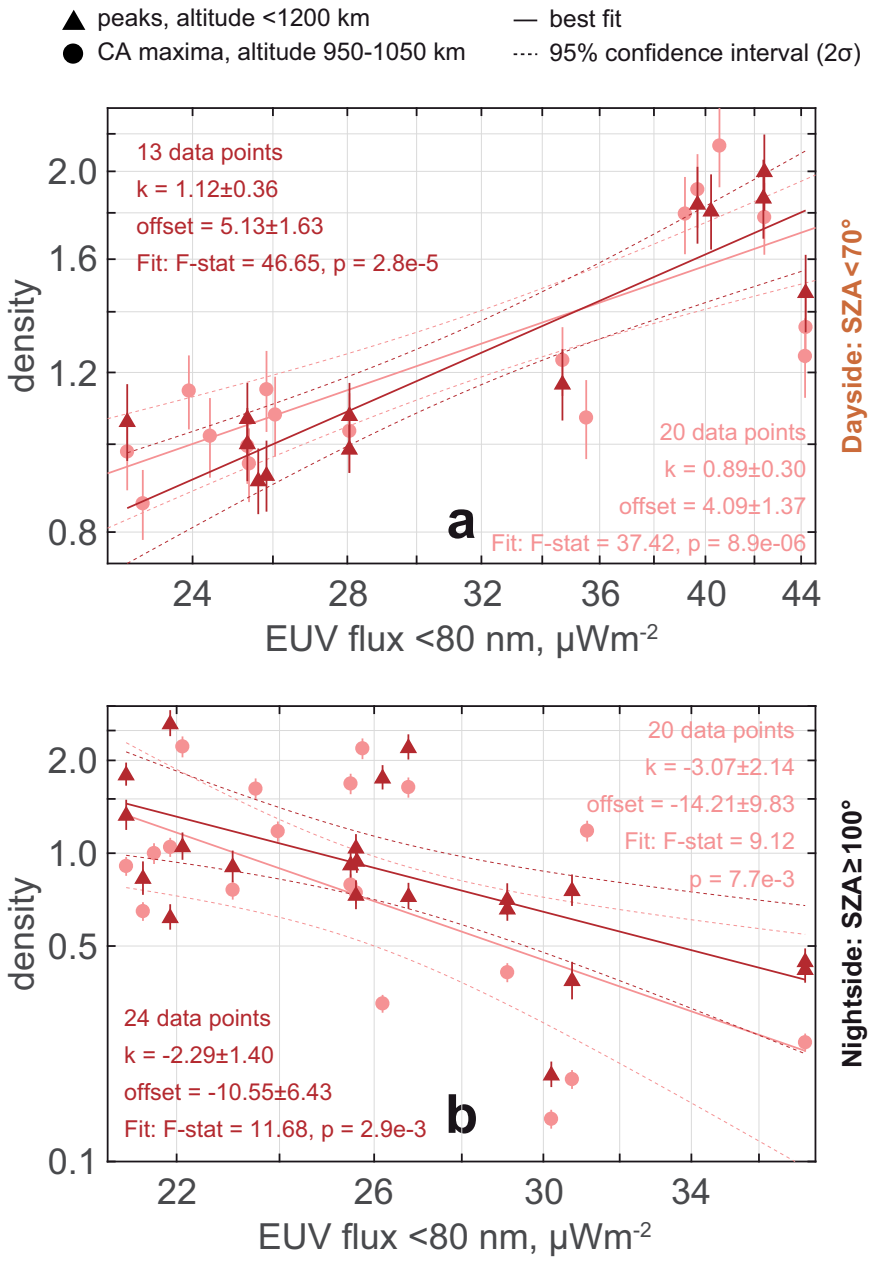

Figure 16. *Normalized positive ion charge density (by SZA on the dayside and median on the nightside) plotted versus integrated EUV flux <80 nm: peak densities (▲) and closest approach maxima (●). Best fits ($\log n = k \log EUV + offset$) are plotted as solid lines, coefficients and statistics summary given in corresponding colours. All error bars, error margins and fit prediction bounds (dashed lines) are* 95% *confidence level (2σ), all axes are logarithmic. Adapted from Paper III.*

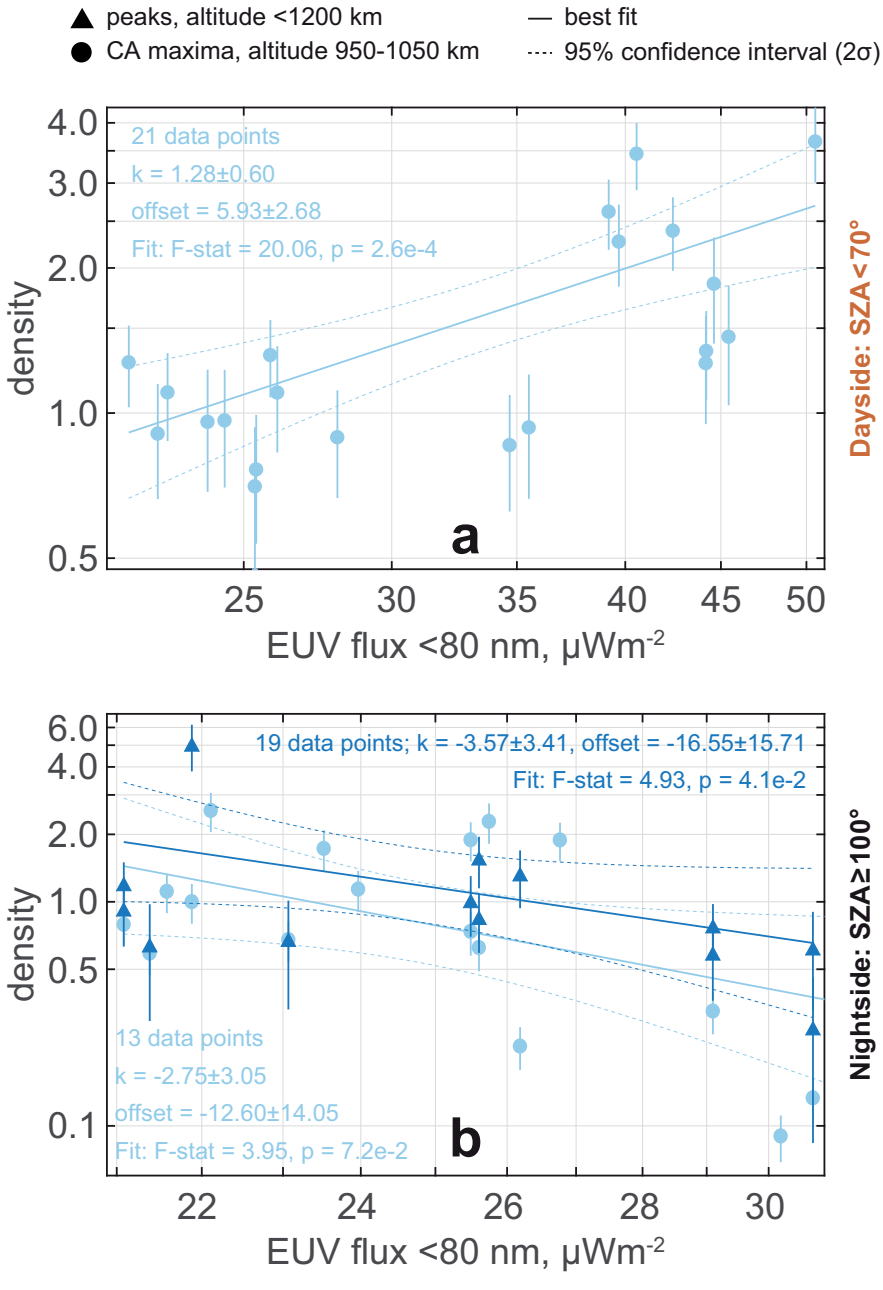

***Figure 17**. Same as **Figure 16**, but for the negative ions/dust grains. Adapted from Paper III.*

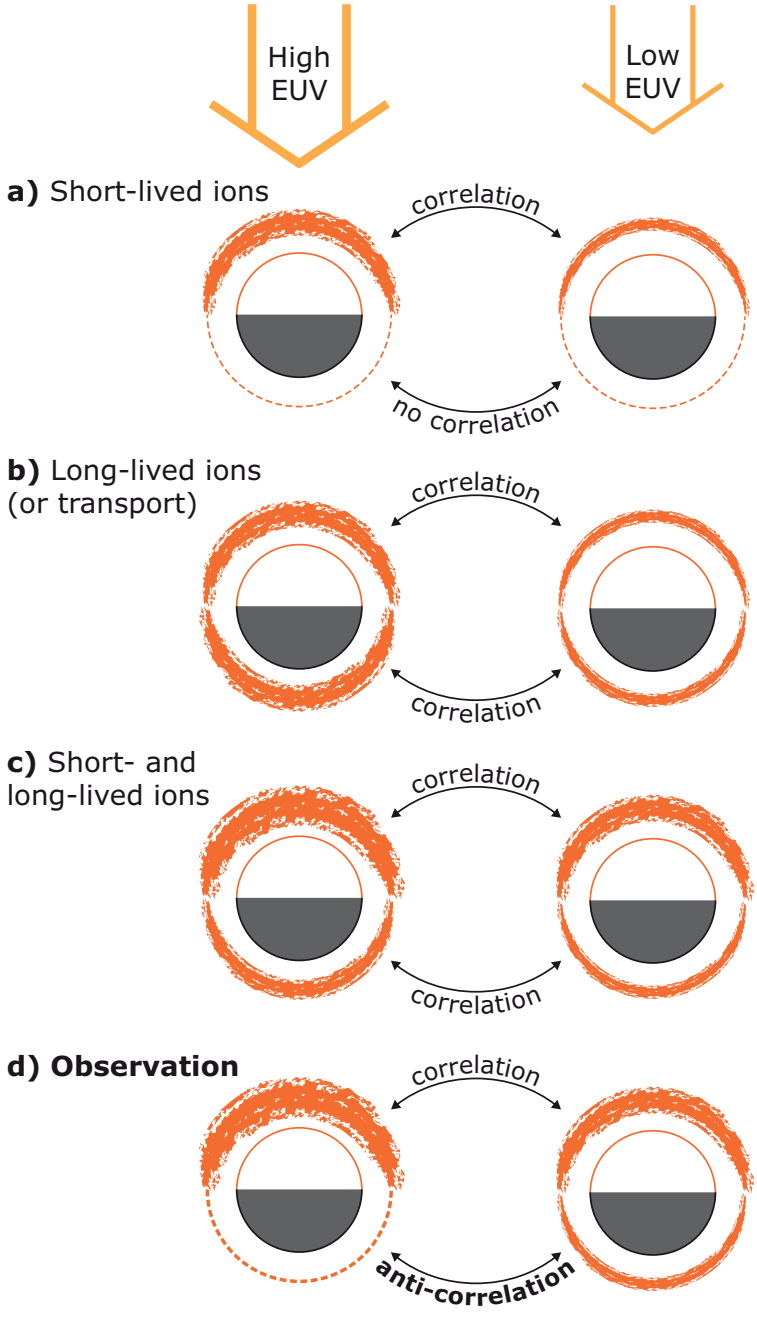

Figure 18. *Different scenarios of the dayside/nightside ion charge density variation due to the solar EUV:* ***a)*** *ionosphere populated primarily by short-lived ions,* ***b)*** *by long-lived ion,* ***c)*** *by a mix of both,* ***d)*** *the observed case. Transport (including super-rotation) has the same effect as long-lived ions (****b****). Thicker lines correspond to higher plasma densities. Adapted from [Paper III].*

Unfortunately this idea will likely remain empirically untested until the next mission to Titan, as the only instrument capable of performing mass spectroscopy of the negative ions, CAPS/ELS, was turned offline before the solar maximum (June 2012.[29]). However, the sharp decrease of the ion charge densities across the dusk region of Titan's ionosphere show the absence of the day to night transport, and the nightside ion column densities across the solar cycle indicate no influences of the thermosphere expansion due to the enhanced EUV flux [Paper III].

3.3 Dust

Dusty plasmas have been observed in the noctilucent clouds and D-region of ionosphere on Earth [*Havnes et al.*, 1996], Enceladus plume and E-ring of Saturn [*Wahlund et al.*, 2005, 2009a; *Morooka et al.*, 2011; *Engelhardt et al.*, 2015], deep ionosphere of Titan [Paper I, II, III] and cometary comas. A dusty plasma is defined by the so-called dusty plasma condition, $r_d \ll d \ll \lambda_D$: the dust grain radius r_d must be small compared to the intergrain distance d, which in turn must be smaller than Debye length λ_D. If the condition is satisfied, the dust particles are coupled and exhibit collective behaviour, otherwise the system is referred to as "dust in plasma" [*Shukla*, 2001; *Morooka et al.*, 2011]. Dust particles in a plasma act like tiny spacecraft: electrons will condense on (attach to) them and charge them negatively in the same way [e.g., *Shukla and Mamun*, 2002; *Horanyi et al.*, 2004; *Wahlund et al.*, 2009a], hence the electron density in a dusty plasma decreases with increasing dust density and grain size. For instance, *Morooka et al.*, 2011 showed that the dusty Enceladus plume is nearly devoid of electrons. Similar electron depletion was also observed in the ionosphere of Titan below 1100 km altitude [Paper I, II]. For a spacecraft in a dusty plasma, the flux of the charged dust must be included in the current balance of the spacecraft potential. At the same time, a measured spacecraft potential may be used as a proxy for the dust grain potential due to similar charging mechanisms, which together with grain size and electron temperature provides constraints for the average grain charge [e.g., *Whipple et al.*, 1985; *Goertz*, 1989; *Horányi et al.*, 2004; *Hill et al.*, 2012; *Engelhardt et al.*, 2015s; Paper I].

Dusty plasma exhibits different properties than "normal" plasma because of the much heavier negative particles (compared to the positive ions). Heavy negatively charged particles have more inertia and are less affected by the electromagnetic forces while still influencing the rest of plasma, how and to what extent depends on the dust grain size distribution. An example is Saturn's

[29] http://saturn.jpl.nasa.gov/news/significantevents/anomalies/

E-ring populated by the dust from Enceladus [*Kurth et al.*, 2006, and references therein]: the velocities of the μm-sized dust particles tend towards Keplerian[30] motion rather than following the corotation of the ambient magnetospheric plasma, while nm-sized particles are pulled along with the latter by strong electric fields [see e.g., *Hsu et al.*, 2013].

In Titan's ionosphere, the dusty plasma condition above is fulfilled globally below 1400 km altitude [Paper II], and the presence of dust grains is marked by the gradual depletion of the electron densities (compared to the positive ion charge density) towards lower altitudes, as the electrons condense on (attach to) the dust grains (**Figure 19**). On the nightside, the electrons are depleted by $\geq 50\%$ at $\sim$1100 km altitude. On the dayside, the depletion of electrons is $\sim 50\%$ at $\sim$900 km altitude (lowest reached by the Cassini spacecraft), and the plasma is expected to be dusty further down [Paper II].

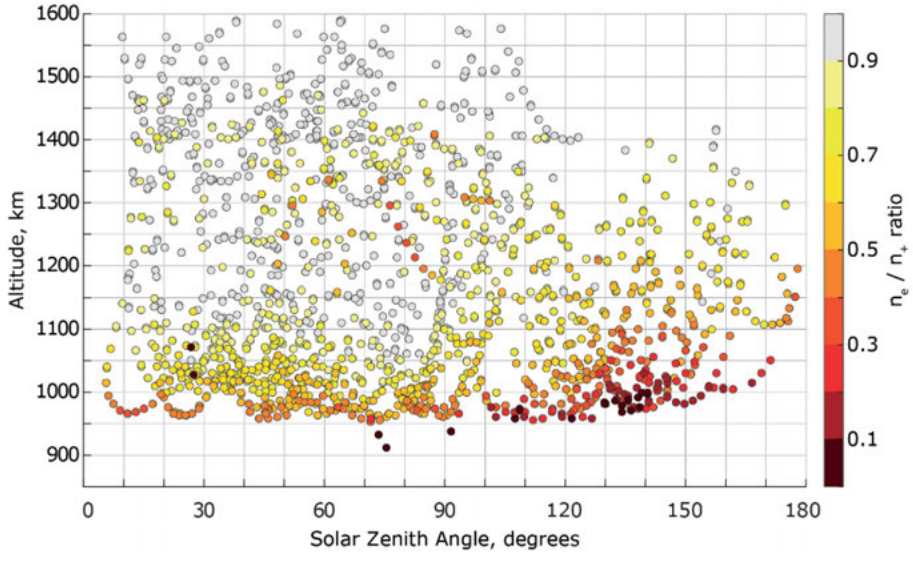

Figure 19. *"Dust map" of Titan's ionosphere – electron to ion charge density ratio (RPWS/LP derived) plotted in altitude and solar zenith angle. Since the dusty plasma condition is satisfied everywhere below 1400 km altitude, the electron depletion ($n_e/n_+ < 0.5$) may be used as an indicator of a dusty plasma.*

Another quirk of the dusty (and generally, ion-ion) plasma is an ion charge density enhancement. The positive ions are estimated to recombine with the negative ions and dust grains a factor $\sim 5-10$ slower than with the free electrons [*Vigren et al.*, 2014]. The slower ion loss results in a boost of the ion charge densities as the electrons deplete. This is visible even in the large scale

[30] Here: governed by gravity

ionosphere map in **Figure 14**: the positive ion charge densities below the primary (EUV-induced) peak line increase sharply as the negative ions become prominent and the electron densities decrease at corresponding altitudes. To really drive this point home though, examples of individual flybys are much more illustrative: **Figure 20** shows the RPWS/LP derived charge densities from two of the flybys (T29 and T56) analysed in Paper II. Note that both positive (**red**) and negative (**blue**) ion/dust grain charge densities increase sharply as the electron densities (**black**) drop in the dusty plasma regions (shaded).

An important result of Paper II is the first empirical estimation of the negative ion/dust grain charge. Dust grain charge have previously been estimated with an application of the dust charging theory as mentioned above. The empirical estimate is obtained by combining the RPWS/LP and CAPS/ELS measurements: the former measures the negative ion/dust grain charge density ($z\_n\_$), the latter – density per charge ($n\_/z\_$), giving the average dust grain charge estimate as

$$\bar{z}_- = \sqrt{\frac{(z_- n_-)_{LP}}{(n_-/z_-)_{ELS}}}\,. \qquad [10]$$

Since the CAPS/ELS and RPWS/LP measure simultaneously (although asynchronously), altitude profiles of $\bar{z}_-$ may be derived, which has been done for T16, T29, T40 and T56 in Paper II, **Figure 21**.

Apparent dust grain radius required to support the derived $\bar{z}_-$ (**Figure 21**) may be calculated assuming a spherical grain in thermal equilibrium:

$$\mathrm{R_{dust}} = \frac{z_- q_e}{4\pi\varepsilon_0 U_D}\,, \qquad [11]$$

where ε_0 is the vacuum permittivity and U_D is the dust potential, which can be approximated by the Cassini spacecraft potential[31] measured by the RPWS/LP. It should be noted that the spherical grain assumption is rather frail because the CAPS/ELS-derived masses for the heaviest psarticles and the estimated R_{dust} give mass densities $\sim 1-6$ kgm-3 (for comparison, solid methane is ~ 500 kgm-3); such low mass densities may be expected of hollow structures like fractal particles[32] [Sittler et al., 2009; Waite et al., 2010; Michael et al., 2011]. For this reason, R_{dust} is referred to as the "apparent" dust radius.

---

[31] The approximation has been validated in the much denser dusty plasma of Enceladus' plume; charging mechanisms other than the thermal equilibrium were also shown to be insignificant [*Engelhardt et al.*, 2015]

[32] Snowflakes are an example of fractal particles, with densities ~2 orders of magnitude smaller than water ice

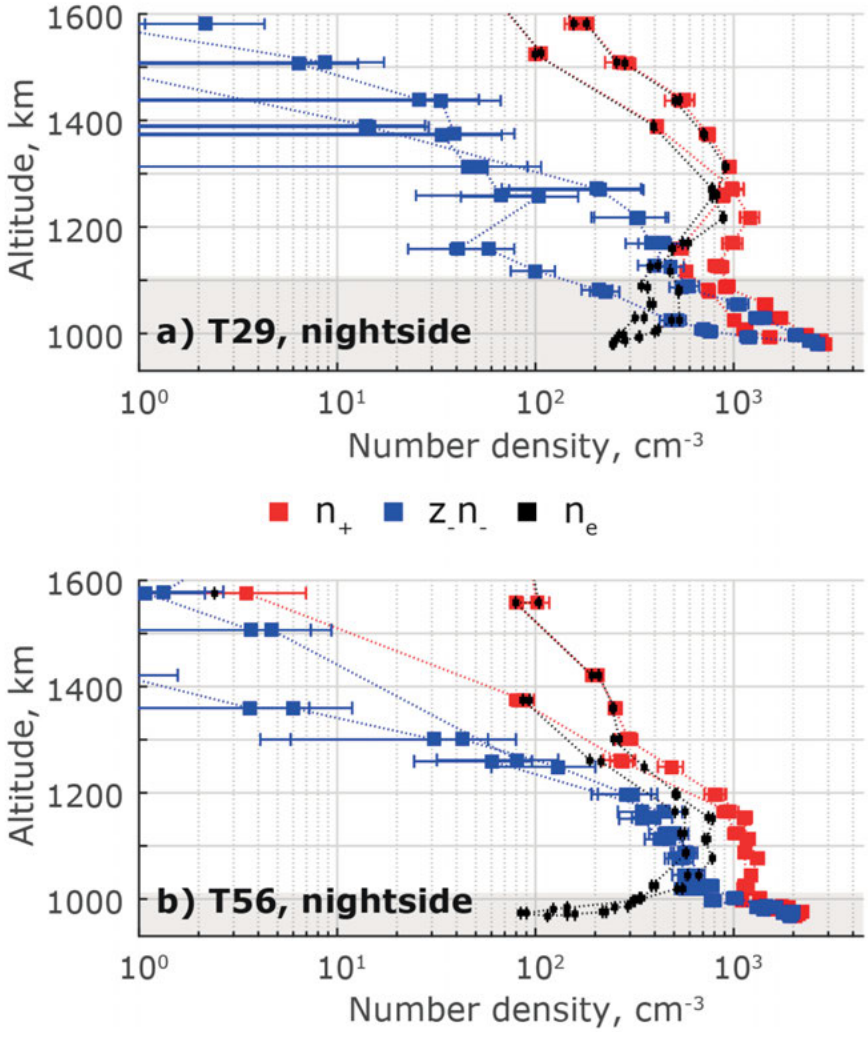

Figure 20. . *RPWS/LP derived* ***positive*** *and* ***negative*** *ion charge densities (log scale) using the method described in Paper II (flybys T29 and T56). Each measurement gives two points, one from* $-4 \rightarrow 0$ *V sweep and one from* $0 \rightarrow -4$ *V. Error bars mark* 95% *confidence intervals. The* ***electron densities*** *are derived directly from the DC ion current* α *in eq. [7] assuming quasineutrality* ($n_e + z_- n_- = n_+$, *with* $2\sigma_\alpha \sim 10^{-5}$ *cm*$^{-3}$*). The shaded areas show the regions of dusty plasma (expected in case of T40). Adapted from Paper II.*

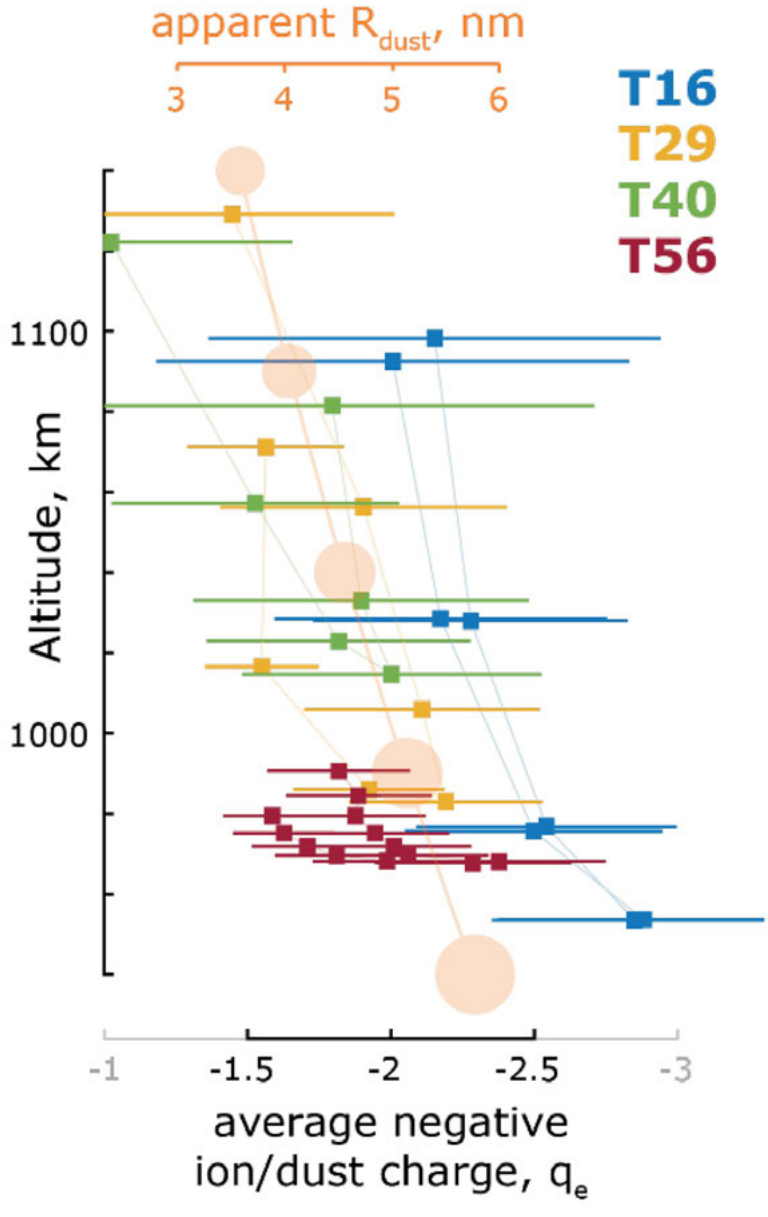

Figure 21. *Estimate of the average charge (**lower axis**) of the negative ions/dust grains (in elementary charges q_e) derived from the combined RPWS/LP and CAPS/ELS measurements for the flybys **T16**, **T29**, **T40** and **T56** (the error bars mark the 95% confidence intervals). The corresponding apparent average dust radius (**upper axis**) is plotted in **orange circles** in the background. Adapted from Paper II.*

3.4 Photoionization modelling

Understanding of the EUV dependencies of the ion charge densities, along with decreasing (increasing) altitude of the positive (negative) ion charge density peaks with the increased solar EUV flux requires ionization and global circulation models. We model the ionization of Titan's dayside and terminator ionosphere in Paper IV to see how the electron (≡ positive ion) production (≡ ionization) rate changes through the solar cycle, which may provide clues about the observed nightside anti-correlation shown in **Figure 16**. The model is based on the measured densities of N_2 (by the INMS) and the < 80 nm EUV flux measured at 1 AU (by TIMED/SEE) and translated (in phase and distance) to Saturn[33]. To account for the variation of the N_2 density altitude profiles with the solar EUV flux (**Figure 22**, see also *Westlake et al.*, 2014s), the N_2 densities are used instead of altitude in plots of the model parameters.

Ionization balance models applied to a few flybys has previously been shown to overestimate the measured densities by a factor of $\lesssim 2$ [e.g., *Vigren et al.*, 2013; *Richard et al.*, 2015]. Including 34 dayside/terminator flybys between TA and T120 we extend the model by *Vigren et al.*, 2013, revealing a previously unnoticed trend: besides the expected dependency on the altitude (i.e., the neutral atmosphere N_2 densities), the recombination ("loss") coefficient α_{eff} exhibits trends with respect to the solar zenith angle (SZA), the EUV flux and the angle to Saturn's corotational plasma RAM[34] direction (**Figure 23**). The SZA dependency is likely due to modelled photoionization diminishing towards terminator with the declining solar illumination, while the measured densities are still affected by the energetic particle ionization. The RAM trend should instead be directly correlated with the ionization by the energetic magnetospheric particles, with 0° corresponding to the RAM side of the ionosphere and 180° to the wake side, an increase towards ~90° agrees with the expected particle precipitation (due to Saturn's magnetic field draping around Titan). The EUV flux has been suggested to affect the photochemistry [Paper III, *Westlake et al.*, 2014], which in turn affects the downward flux of the heavier particles.

---

[33] The phase translation achieves only 600″ accuracy for the orbital position of Saturn due to the ephemeris prediction algorithm utilizing a 2-body model, this accuracy proves sufficient as was shown in **Figure 4**.

[34] The RAM angle is the angle between the direction of the incoming corotational plasma (i.e., anti-parallel to the corotational plasma flow) and the direction (position vector) of the spacecraft. The concept is the same as the SZA and is used in the similar fashion to distinguish between the side of Titan facing the incoming flow of particles (RAM side) and the side of the flow wake.

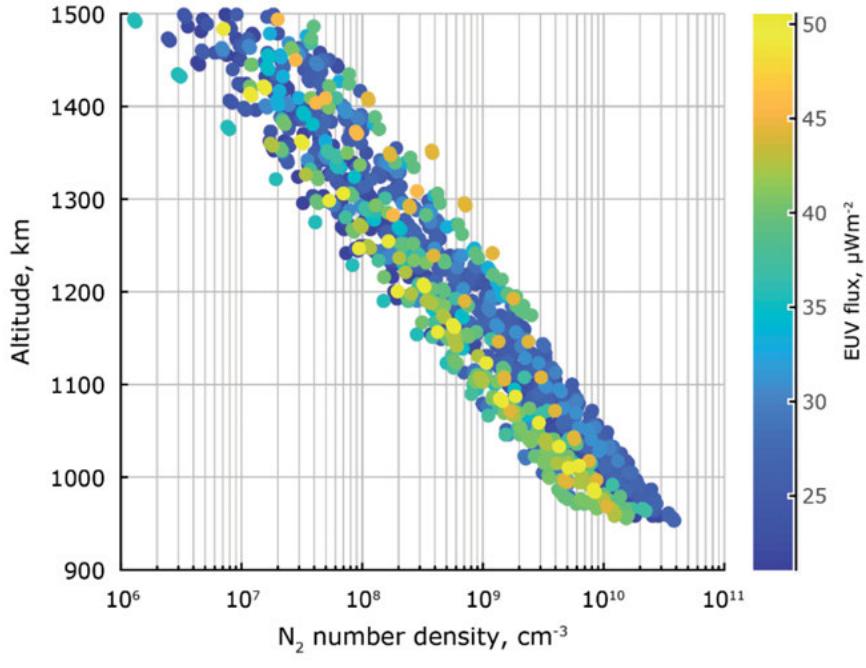

Figure 22. *Variation of the N_2 density altitude profiles with the solar EUV flux (colour-coded). At higher altitudes, the N_2 densities are enhanced by the thermosphere expanding with increasing EUV flux, but at lower altitudes the densities are diminished [see also Westlake et al., 2014], consistent with an EUV-induced change in the photochemistry [Paper III, Westlake et al., 2014]. Adapted from Paper IV.*

To mitigate the absence of the negative ions in the model, we calculate the loss rate coefficient α_{eff} using $\sqrt{n_e n_+}$ rather than n_e^2 as was done in *Vigren et al.*, 2013 (which is a good approximation for the regions with the negative ions significantly fewer than the electrons). However, the coefficient from *Vigren et al.*, 2013 is based on four nearly identical flybys and therefore does not account for the variability of Titan's ionosphere. This is evident in the comparison between the two, **Figure 24**, where the coefficients from *Vigren et al.*, 2013 have larger values (filled triangles) compared to the current model (empty triangles). The pink shaded area represents the *Vigren et al.*, 2013 estimate based on the ion composition and electron temperatures, which is still lower than the values from the current model but the improvement is none the less clear.

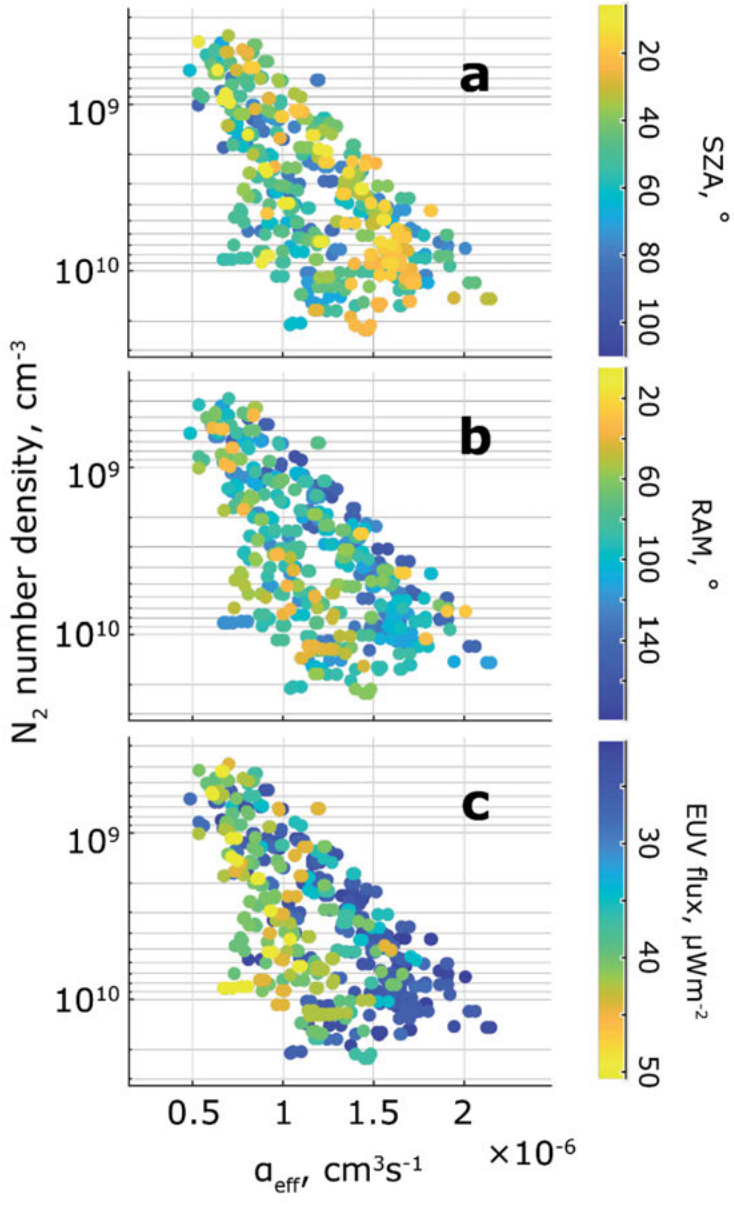

Figure 23. *Estimated loss rate coefficients calculated as* $\alpha_{eff} \approx P_e(n_e n_+)^{-1}$*, plotted versus* N_2 *densities with colour-coded SZA (**a**), RAM (**b**) and the solar EUV flux (**c**). SZA* $< 70°$ *corresponds to the dayside,* $70° <$ *SZA* $< 110°$ *corresponds to the terminator. The RAM angle is* $0°$ *on the upstream side of Titan (ram side) and* $180°$ *is on the downstream side (wake side). Adapted from Paper IV.*

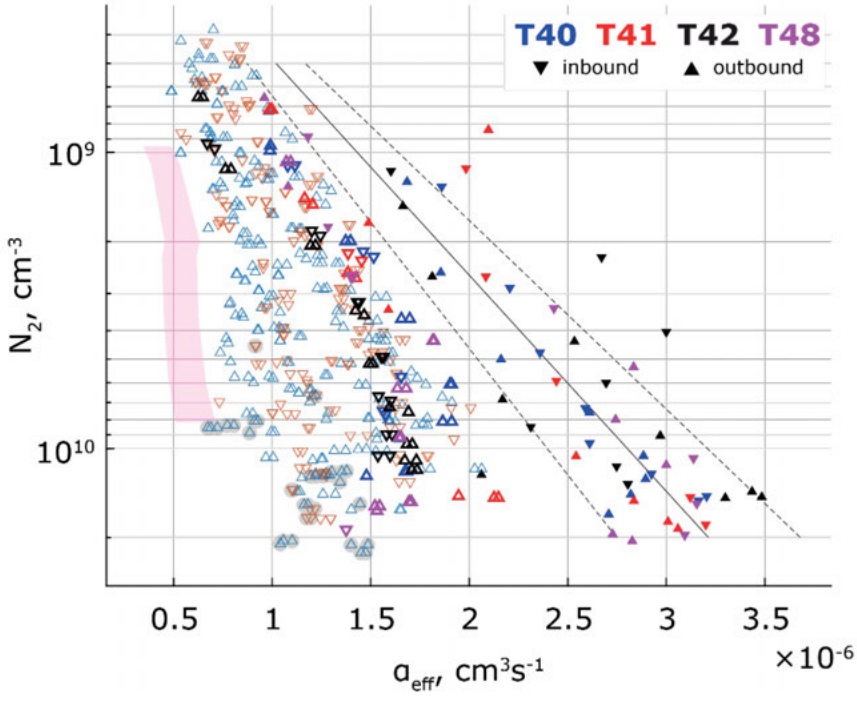

Figure 24. *Comparison of the ion-electron recombination coefficient from Vigren et al., 2013 (filled triangles) and the one calculated using* $\sqrt{n_e n_+}$ *(empty triangles). Data points from the four flybys used in Vigren et al., 2013 matched in color, the rest are drawn in blue (inbound) and red (outbound). The best fit* $\pm 1\sigma$ *for the Vigren et al., [2013] dataset is shown as solid and dashed black lines. The pink shaded area represents the* α_{eff} *estimated by Vigren et al., [2013] based on the measured ion composition and electron temperatures. Gray circles at higher* N_2 *densities mark the points with* $z\_n\_/n_e > 1$

In conclusion, the loss rate coefficient dependencies on the SZA, RAM and EUV flux are shown to be statistically significant and the variations of Titan's ionosphere with respect to these parameters must be accounted for in the models. The variations with respect to the SZA may be explained by the declining photoionization against the background ionization by the energetic magnetospheric particles, the latter is directly correlated with the RAM angle and the EUV dependency suggests a photochemistry changing with the sunlight intensity.

4 Summary of publications

4.1 Paper I

Title: Negative ion densities on the ionosphere of Titan – Cassini RPWS/LP results

Authors: Shebanits O., Wahlund J.-E., Mandt K., Ågren K., Edberg N.J.T., Waite J.H.

Journal: Planetary and Space Science

Status: Published

Summary:

In this paper we study the charge density distributions of the electrons, positive and negative ions in Titan's ionosphere. The study includes 47 flybys with closest approach below 1400 km altitude, between TA (Oct 2004) and T84 (July 2012). Mapping the charge densities to altitude and solar zenith angle revealed a significant amount of the negative ions, particularly on the nightside and below altitudes of 1000 km, accompanied by substantial depletion of free electrons ($n_e/n_+ \sim 0.1 - 0.7$). The negative ions effectively extended the known levels of ionization in Titan's ionosphere, which were previously based on the electron densities.

The altitudes of the main ionospheric peak are found to increase towards the terminator region ($70° < \mathrm{SZA} < 110°$), in agreement with the earlier measurements. The negative ion charge densities increase exponentially with decreasing altitudes (down to the lowest flown altitudes of 880 km), reaching up to 2500 cm^{-3}, compared to the positive ion densities reaching 4200 cm^{-3}. The electron depletion in the nightside ionosphere and large negative ion charge densities imply dusty plasma: the dominant negative charge carriers are the heavy negative ions, with $10^4 - 10^6$ ions/Debye cube. Negative ions are predicted to have $1 - 2$ charges based on thermal equilibrium with Cassini spacecraft potential as proxy for the dust potential.

Lower negative ion charge densities around the ecliptic polar regions as compared to the ecliptic equatorial region are another confirmation of the importance of the solar EUV for the ion production. Magnetospheric plasma impacts on the ionization was also investigated but no correlation was identified with the used dataset.

Errata:

Typo in eq. A11: $-\frac{4}{eA_{LP}}$ should not have the minus sign.

My contribution to Paper I:

I performed the RPWS/LP ion data analysis and had the main responsibility for writing the paper.

4.2 Paper II

Title: Ion and aerosol precursor densities in Titan's ionosphere: A multi-instrument case study

Authors: Shebanits, O., Wahlund, J.-E., Edberg, N. J. T., Crary, F. J., Wellbrock, A., Andrews, D. J., Vigren, E., Desai, R. T., Coates, A. J., Mandt, K. E., Waite, J. H.

Journal: Journal of Geophysical Research: Space Physics

Status: Published

Summary:

In this case study we combine independent *in-situ* measurements of plasma charge densities (by RPWS/LP) and ion mass distributions (by CAPS/ELS, CAPS/IBS and INMS) of Titan's ionosphere from flybys T16, T29, T40 and T56. The dataset is used to develop a Titan-specific method for a detailed analysis of the RPWS/LP ion measurements that further constrains the ion charge densities, and produce the first empirical estimate of the average charge of negative ions /dust grains. Part of this method yields altitude profiles of mean ion masses that include heavier ion species (essentially extending the mean ion masses measured by the INMS), which may be derived for any flyby, even where the CAPS data is unavailable.

The charge densities derived with the new method reveal a presence of an ion-ion (dusty) plasma below ~1100 km altitude with charge densities exceeding the primary (EUV) ionization peak values by a factor ≥ 2 in the terminator and nightside ionosphere ($n_e/n_i \leq 0.1$). On the dayside, the depletion of free electrons reaches 50% at the closest approach ($n_e/n_i < 0.5$ at 1000 km altitude). Together with a fulfilled dusty plasma condition this indicates that the dayside ionosphere also has a region of ion-ion (dusty) plasma, with peak below 900 km altitude; the dusty plasma is therefore a global phenomenon in Titan's ionosphere.

The combined dataset is also used to estimate the average charge of the negative ions/dust grains (≥ 1000 amu) between -2.5 and -1.5 elementary charges, increasing toward lower altitudes.

Errata:

Typos in eq:s 6-8, $\frac{m_{eff-}}{Z_-}$ should be replaced by m_{eff-}, and in eq:s 6 and 7, r_{lp} should be replaced by r_{lp}^2.

My contribution to Paper II:

I planned the study, refined and performed the RPWS/LP ion data analysis and had the main responsibility for writing the paper.

4.3 Paper III

Title: Titan's ionosphere: a survey of solar EUV influences

Authors: Shebanits O., Vigren E., Wahlund J.-E., Holmberg M.K.G., Morooka M., Edberg N.J.T., Mandt K.E., Waite J.H.

Journal: Journal of Geophysical Research: Space Physics

Status: Published

Summary:

In this paper we study the effects of the solar EUV on positive ions and negative ions/dust grains in Titan's ionosphere, over the course of almost 12 years. The dataset includes 78 flybys between TA (Oct 2004) and T120 (June 2016) with closest approach below 1400 km altitude. The results show that the solar EUV flux < 80 nm has a strong impact on the ion and dust ion grain charge densities: a factor ~2 *increase* of the dayside/terminator charge densities and a factor ~4 *decrease* of the nightside charge densities is observed during the solar maximum (as compared to the solar minimum). One explanation is that the higher EUV flux changes the ionospheric photochemistry as to remove the positive and negative ions/dust grains from the region of observation. Interpretation of this phenomenon requires knowledge of the ion-electron pair production rate which is the aim of our next study. For now the conclusion is that the higher solar EUV flux may speed up the ion-ion/dust grain chemistry by enhancing the plasma densities, which should have implications for the aerosol production below the altitudes reachable by the Cassini spacecraft.

The position of Titan in the Kronian magnetosphere was observed to have an unexpected impact on the nightside plasma densities at ~1000 km altitude, with higher values in the sunward magnetosphere compared to the magnetotail. The observations are consistent with the enhancement of the particle flux intensity from the tail towards sunward magnetosphere, detected by the ENA instrument [*Mitchell et al.*, 2009]. The specific altitude of these variations is in agreement with the peak ionization by the magnetospheric

particle precipitation [*Cravens et al.*, 2008; Fig. 11.25 in *Galand et al.*, 2014 and references therein].

The presented observations also strongly imply that the Chapman theory is not applicable for Titan's ionosphere below 1200 km altitude.

My contribution to Paper III:

I planned the study, performed the RPWS/LP ion data analysis, updated the photoelectron current correction and had the main responsibility for writing the paper.

4.4 Paper IV

Title: Photoionization modelling of Titan's dayside ionosphere

Authors: Shebanits O., Vigren E., Wahlund J.-E., Edberg N.J.T., Cui J., Galand, M., Mandt K.E., Waite J.H.

Journal: The Astrophysical Journal

Status: manuscript in preparation

Summary:

Photoionization models of Titan's ionosphere tend to overestimate the electron (positive ion) charge densities by a factor of ~2, but are typically based on a few flybys. In this paper we model Titan's ionosphere based on the measurements of the neutral atmosphere and the solar EUV flux and compare the model with the plasma measurements. Our results show that the plasma density overestimation by photoionization models depends on the solar zenith angle, corotational plasma RAM angle and solar EUV flux. We produce an empirical fit of the loss rate coefficient to the N_2 number densities, solar EUV flux, solar zenith angle and corotational plasma RAM angle for use in the modelling of Titan's ionosphere and show these trends to be statistically significant. The trends may be explained by the decreasing solar ionization against the background ionization by the energetic particles (SZA trend), particle ionization (RAM trend) and chemistry affected by the sunlight conditions (EUV trend).

My contribution to Paper IV:

I performed the RPWS/LP ion data analysis, participated in the study planning, developed the ionospheric model and had the main responsibility for writing the paper.

5 Sammanfattning på svenska

Denna avhandling fokuserar på utforskningen av Saturnus måne Titans jonosfär. Titan (2575 km radie) är den enda kända måne i solsystemet som har en fullständigt utvecklad atmosfär och jonosfär som på grund av månens relativt låga gravitation sträcker sig till nästan 2 Titanradier (ca 2200 km höjd). En jonosfär är joniserad gas och bildas i en atmosfär (oftast övre delar) som utsätts för joniserande strålning (UV och EUV ljus, kosmisk strålning eller partiklar med tillräckligt hög energi). Titans jonosfär har under senare år blivit känd för sin komplexa organiska kemi och tros likna den tidiga Jordens jonosfär. Utforskning av Titans jonosfär är högst relevant i frågan om livets uppkomst. Redan 1953 har man visat att komplexa organiska molekyler (i det fallet, aminosyror) kan bildas i en joniserad gasblandning av ammoniak, metan, vattenånga och väte; moderna experiment har visat att aminosyror kan bildas även i en gasblandning av koldioxid, metan och kväve (alltså utan vatten) – produktion av livets byggstenar behöver således inte vara begränsad till vattenpölar på marken. In-situ mätningarna (alltså mätningar på plats) har avslöjat att Titans jonosfär består av kväve (97%), metan ($< 2.7\%$) och komplexa organiska molekyler (kolväten och nitriler), de sista tros bilda stoftkorn (aerosoler) i Titans oranga dis. Några aminosyror har man inte funnit i gasform (Titans atmosfär har endast spårmängder av vatten) men det är möjligt att de produceras på marken där kopplingar till Titans underjordiska hav kan finnas. Jonosfärsstudier utgör grunden för ett ramverk av dess komplexa organiska kemi som kan bidra till vårt kunskap av liknande processer i tidiga Jordens atmosfär. I denna avhandling granskar vi Titans jonosfär från ett rymdperspektiv och undersöker dess tyngre plasmakomponenter, dvs positiva joner och negativa joner/stoftkorn.

Data som används kommer från instrumenten ombord på rymdsonden Cassini som har varit i omloppsbana kring Saturnus från den 1:a juli 2004 till den 15:e september 2017. Huvudsakligen är data från Langmuirsonden (byggd av Institutet för rymdfysik i Uppsala) med stödjande data från partikelinstrument INMS (byggd av NASA), CAPS/IBS (byggd av SWRI) och CAPS/ELS. Langmuirsonden mäter strömmen av laddade partiklar i plasma (joniserad gas). För att undersöka energin hos de laddade partiklarna ges sonden en elektrisk spänning (typiskt ± 4 V i Titans jonosfär) relativt omgivningen. Vi kan använda dessa observationer för att (med hjälp av massfördelningar från partikelinstrumenten) räkna fram partikeltätheter för

jonosfärens komponenter: elektroner, positiva joner och eventuella negativa joner/stoftpartiklar.

Cassinis största upptäckt i Titans jonosfär är negativa joner, upp till 13800 atommassor per laddning, som består av klusterjoner och stoftpartiklar. I Artikel I har vi med hjälp av mätdata från Langmuirsonden och INMS visat att dessa negativa joner utgör en signifikant del av Titans jonosfär och på nattsidan är till antalet jämförbara med eller fler än elektronerna (elektronerna kondenserar på stoft). Jonosfärsplasma i sådana regioner kallas stoftplasma – det vill säga plasma där de negativt laddade stoftpartiklarna ersätter elektronerna som primära bärare av negativ laddning. I Artikel II använder vi synkroniserade mätningar från Langmuirsonden (samtliga positiva joner, negativa joner och negativt laddade stoftpartiklar) och partikelinstrumenten INMS (positiva joner < 100 amu), CAPS/IBS (positiva joner $\lesssim 1100$ amu) och CAPS/ELS (negativa joner och stoftpartiklar, $\lesssim 13800$ amu/laddning) för att ta fram en analysmetod för data från Langmuirsonden som är specifik för Titans jonosfär, med syftet att förbättra noggrannheten av framtagna jontätheterna. Med den nya metoden visar vi att stoftplasma är ett globalt fenomen i Titans jonosfär under $900 - 1100$ km höjd och uppskattar experimentellt stoftpartiklarnas medelladdning att vara mellan -1.5 och -2.5 elementarladdningar. Stoftplasma är en jon-jon plasma och har annorlunda egenskaper än vanlig jon-elektron plasma, bland annat blir rekombinationen av de positivt och negativt laddade partiklarna mycket långsammare (ca 5 gånger) än i jon-elektron plasma (negativt laddat stoft är mycket trögare än elektroner). Detta innebär mindre förlust av laddade partiklar och tillåter dess partikeltätheter i stoftplasma att växa upp till $2 - 3$ gånger så högt som i jon-elektron plasma (in-situ uppmätta tätheterna är upp till 10000 cm^{-3} i stoftplasma jämfört med upp till $4000 - 6000$ cm^{-3} i jon-elektronplasma). Strukturen av Titans jonosfär blir således: en jonisationsdriven del med jon-elektron plasma ner till ca $900 - 1100$ km höjd (lägre på dagsidan) och en kemidriven del med stoftplasma från $900 - 1100$ km höjd och neråt.

Efter att Cassini har samlat in mätdata från Titans jonosfär under längre tid än en hel solcykel (11 år) har det blivit möjligt att studera effekter av solaktivitet på jonosfärsplasma. I Artikel III visar vi hur partikeltätheterna ökar med en faktor 2 från solminimum till solmaximum i jonosfärens dagsida samt underligt nog avtar med en faktor $3 - 4$ på nattsidan. En möjliga förklaringar är förändrad fotokemi som flyttar både de positiva jonerna och de negativa jonerna/stoftpartiklarna utanför (in-situ) observerbara områden. Artikel IV syftar till att följa upp dessa resultat med en jonisationsmodell baserad på mätningar av EUV-strålning och densiteten för kväve som representerar det dynamiska neutrala atmosfären. Tidigare modeller hade stadigt överskattat partikeltätheter av Titans jonosfärsplasma men baserades på få förbiflygningar. Genom att inkludera data från samtliga tillgängliga förbiflygningar (dagsidan och terminator, totalt 34) kunde vi visa att överskattningen minskar med minskad solbelysningsnivå (solzenitvinkel).

Överskattningen minskar även med ökad EUV-strålning, något som kan bero på fotokemi som förändras med högre EUV intensitet, och är högre på Titans ledande sida i omlopsbanan (relaterat till inflödet av energirika partiklar från Saturnus magnetosfär). Vi tar fram en empirisk anpassning av förlustkoefficienten för användning i fotojonisationsmodeller av Titans jonosfär.

Vår forskning har bidragit till förståelse av Titans jonosfär (och stoftplasma i denna jonosfär), dess struktur och dynamik. Metoder som vi har utvecklat för analys av data från Cassinis Langmuirsond kan vara användbara för andra Langmuirsonder i liknande plasmamiljöer med stoftplasma.

6 Acknowledgements

It is easy to take for granted the great many people that are involved in one's work. The journey that has been this PhD project wouldn't be possible without the many awesome persons surrounding me.

First and foremost I want to express my truly astronomical gratitude to my best friend and life partner, Kateryna, who were there to share my excitement when I started this project, supported me throughout and helped me shoulder many challenges in the end. You have always been and always will be my beacon.

My supervisor, mentor and in many ways (perhaps even too many) most like-minded person I have met, Jan-Erik Wahlund, to whom I have looked up from the time I awkwardly stumbled in looking for a master thesis project, who have shown me the awesome world of Space Science and guided me on this amazing path of exploration and discovery. From the bottom of my heart, thank you for making my childhood dream come true. My co-supervisors, Wolf Dietrich Geppert and Olle Björneholm, and my newest co-supervisor (vice-supervisor?), Erik Vigren, thank you all for your wisdom, it provided a much needed perspective.

I want to thank my senior colleagues who have been unofficially supervising me. Anders Eriksson, for sharing your knowledge and unending optimism. Michiko Morooka, for showing me an elegant way to code. David Andrews, for helping me smooth out the edges (and the occasional dads-wth-kids hangouts). Mats André, for his most meticulous attention to detail and extensive knowledge about our worst enemy, bureaucracy. A big round of thanks to our engineers, Lennart Åhlén and Sven-Erik Jansson, whose wordplay jokes could keep me giggling for days, and to our administrators Jenny Andersson and her predecessor Ingrid Wahlberg for always taking care of me and my endless troubles with the infrastructure.

I also want to thank my fellow PhD students: my partners in crime Mika Holmberg and Cecilia Norgren who always kept the spirits up, my office roomie Ilka Engelhardt for being refreshingly straight-forward and joining me in my rebellion against the princesstårta, my fellow Pokémon trainer Andreas Johlander, Fredrik Johansson for his healthy skepticism, Elin Eriksson and Elias Odelstad for bouncing ideas.

7 Bibliography

Ågren, K. et al. (2007), On magnetospheric electron impact ionisation and dynamics in Titan's ram-side and polar ionosphere–a Cassini case study, *Ann. Geophys.*, *25*(11), 2359–2369, doi:10.5194/angeo-25-2359-2007.

Ågren, K., J. E. Wahlund, P. Garnier, R. Modolo, J. Cui, M. Galand, and I. Müller-Wodarg (2009), On the ionospheric structure of Titan, *Planet. Space Sci.*, *57*(14–15), 1821–1827, doi:10.1016/j.pss.2009.04.012.

Ågren, K. et al. (2011), Detection of currents and associated electric fields in Titan's ionosphere from Cassini data, *J. Geophys. Res. Sp. Phys.*, *116*(4), A04313, doi:10.1029/2010JA016100.

Ågren, K., N. J. T. Edberg, and J. E. Wahlund (2012), Detection of negative ions in the deep ionosphere of Titan during the Cassini T70 flyby, *Geophys. Res. Lett.*, *39*(10), n/a-n/a, doi:10.1029/2012GL051714.

Aharonson, O., A. G. Hayes, P. O. Hayne, R. M. Lopes, A. Lucas, and J. T. Perron (2014), Titan's surface geology, in *Titan*, edited by I. Muller-Wodarg, C. A. Griffith, E. Lellouch, and T. E. Cravens, pp. 63–101, Cambridge University Press, Cambridge.

Barjatya, A., and C. M. Swenson (2006), Observations of triboelectric charging effects on Langmuir-type probes in dusty plasma, *J. Geophys. Res. Sp. Phys.*, *111*(10), A10302, doi:10.1029/2006JA011806.

Béghin, C., C. Sotin, and M. Hamelin (2010), Titan's native ocean revealed beneath some 45 km of ice by a Schumann-like resonance, *Comptes Rendus - Geosci.*, *342*(6), 425–433, doi:10.1016/j.crte.2010.03.003.

Bird, M. ~K., R. Dutta-Roy, S. ~W. Asmar, and T. ~A. Rebold (1997), Detection of Titan's Ionosphere from Voyager 1 Radio Occultation Observations, *Icarus*, *130*(2), 426–436, doi:10.1006/icar.1997.5831.

Coates, A. J., F. J. Crary, G. R. Lewis, D. T. Young, J. H. Waite, and J. C. Sittler (2007), Discovery of heavy negative ions in Titan's ionosphere, *Geophys. Res. Lett.*, *34*(22), L22103, doi:10.1029/2007GL030978.

Coates, A. J., A. Wellbrock, G. R. Lewis, G. H. Jones, D. T. Young, F. J. Crary, and J. H. Waite (2009), Heavy negative ions in Titan's ionosphere: Altitude and latitude dependence, *Planet. Space Sci.*, *57*(14–15), 1866–1871, doi:10.1016/j.pss.2009.05.009.

Coates, A. J., A. Wellbrock, G. R. Lewis, G. H. Jones, D. T. Young, F. J. Crary, J. H.

Waite, R. E. Johnson, T. W. Hill, and E. C. Sittler Jr. (2010a), Negative ions at Titan and Enceladus: recent results, *Faraday Discuss.*, *147*, 293, doi:10.1039/c004700g.

Coates, A. J., G. H. Jones, G. R. Lewis, A. Wellbrock, D. T. Young, F. J. Crary, R. E. Johnson, T. A. Cassidy, and T. W. Hill (2010b), Negative ions in the Enceladus plume, *Icarus*, *206*(2), 618–622, doi:10.1016/j.icarus.2009.07.013.

Coustenis, A. et al. (2007), The composition of Titan's stratosphere from Cassini/CIRS mid-infrared spectra, *Icarus*, *189*(1), 35–62, doi:10.1016/j.icarus.2006.12.022.

Coustenis, A., E. Lellouch, B. Sicardy, and H. Roe (2010), Earth-based perspective and pre-cassini-huygens knowledge of titan, in *Titan from Cassini-Huygens*, edited by R. H. Brown, J.-P. Lebreton, and J. H. Waite, pp. 9–34, Springer Netherlands, Dordrecht.

Crary, F. J., B. A. Magee, K. Mandt, J. H. Waite, J. Westlake, and D. T. Young (2009), Heavy ions, temperatures and winds in Titan's ionosphere: Combined Cassini CAPS and INMS observations, *Planet. Space Sci.*, *57*(14–15), 1847–1856, doi:10.1016/j.pss.2009.09.006.

Cravens, T. E., I. P. Robertson, S. A. Ledvina, D. Mitchell, S. M. Krimigis, and J. H. Waite (2008), Energetic ion precipitation at Titan, *Geophys. Res. Lett.*, *35*(3), L03103, doi:10.1029/2007GL032451.

Cravens, T. E. et al. (2009), Model-data comparisons for Titan's nightside ionosphere, *Icarus*, *199*(1), 174–188, doi:10.1016/j.icarus.2008.09.005.

Cravens, T. E., R. V. Yelle, J. E. Wahlund, D. E. Shemansky, and A. F. Nagy (2010), Composition and structure of the ionosphere and thermosphere, in *Titan from Cassini-Huygens*, pp. 259–295, Springer Netherlands, Dordrecht.

Cui, J., M. Galand, R. V. Yelle, V. Vuitton, J. E. Wahlund, P. P. Lawas, I. C. F. Müller-Wodarg, T. E. Cravens, W. T. Kasprzak, and J. H. Waite (2009), Diurnal variations of Titan's ionosphere, *J. Geophys. Res. Sp. Phys.*, *114*(6), A06310, doi:10.1029/2009JA014228.

Cui, J., M. Galand, R. V. Yelle, J. E. Wahlund, K. Agren, J. H. Waite, and M. K. Dougherty (2010), Ion transport in Titan's upper atmosphere, *J. Geophys. Res. Sp. Phys.*, *115*(6), A06314, doi:10.1029/2009JA014563.

Edberg, N. J. T., J. E. Wahlund, K. Ågren, M. W. Morooka, R. Modolo, C. Bertucci, and M. K. Dougherty (2010), Electron density and temperature measurements in the cold plasma environment of Titan: Implications for atmospheric escape, *Geophys. Res. Lett.*, *37*(20), n/a-n/a, doi:10.1029/2010GL044544.

Edberg, N. J. T., K. Gren, J. E. Wahlund, M. W. Morooka, D. J. Andrews, S. W. H. Cowley, A. Wellbrock, A. J. Coates, C. Bertucci, and M. K. Dougherty (2011), Structured ionospheric outflow during the Cassini T55T59 Titan flybys, *Planet. Space Sci.*, *59*(8), 788–797, doi:10.1016/j.pss.2011.03.007.

Edberg, N. J. T., D. J. Andrews, O. Shebanits, K. Ågren, J. E. Wahlund, H. J.

Opgenoorth, T. E. Cravens, and Z. Girazian (2013), Solar cycle modulation of Titan's ionosphere, *J. Geophys. Res. Sp. Phys.*, *118*(8), 5255–5264, doi:10.1002/jgra.50463.

Edberg, N. J. T. et al. (2015), Effects of Saturn's magnetospheric dynamics on Titan's ionosphere, *J. Geophys. Res. A Sp. Phys.*, *120*(10), 8884–8898, doi:10.1002/2015JA021373.

Engelhardt, I. A. D., J. E. Wahlund, D. J. Andrews, A. I. Eriksson, S. Ye, W. S. Kurth, D. A. Gurnett, M. W. Morooka, W. M. Farrell, and M. K. Dougherty (2015), Plasma regions, charged dust and field-aligned currents near Enceladus, *Planet. Space Sci.*, *117*, 453–469, doi:10.1016/j.pss.2015.09.010.

Engwall, E. (2006), Cold magnetospheric plasma flows: Properties and interaction with spacecraft, Uppsala University.

Engwall, E., A. I. Eriksson, M. André, I. Dandouras, G. Paschmann, J. Quinn, and K. Torkar (2006), Low-energy (order 10 eV) ion flow in the magnetotail lobes inferred from spacecraft wake observations, *Geophys. Res. Lett.*, *33*(6), L06110, doi:10.1029/2005GL025179.

Eriksson, A. I., and J. E. Wahlund (2006), Charging of the Freja satellite in the Auroral Zone, *IEEE Trans. Plasma Sci.*, *34*(5 II), 2038–2045, doi:10.1109/TPS.2006.883373.

Eriksson, A. I. et al. (2006), Electric field measurements on Cluster: comparing the double-probe and electron drift techniques, *Ann. Geophys.*, *24*(1), 275–289, doi:10.5194/angeo-24-275-2006.

Fahleson, U., C. G. F??lthammar, and A. Pedersen (1974), Ionospheric temperature and density measurements by means of spherical double probes, *Planet. Space Sci.*, *22*(1), 41–66, doi:10.1016/0032-0633(74)90122-6.

Fulchignoni, M. et al. (2005), In situ measurements of the physical characteristics of Titan's environment, *Nature*, *438*(7069), 785–791, doi:10.1038/nature04314.

Galand, M., A. J. Coates, T. E. Cravens, and J.-E. Wahlund (2014), Titan's ionosphere, in *Titan*, edited by I. Muller-Wodarg, C. A. Griffith, E. Lellouch, and T. E. Cravens, pp. 376–418, Cambridge University Press, Cambridge.

Garnier, P. et al. (2009), Titan's ionosphere in the magnetosheath: Cassini RPWS results during the T32 flyby, *Ann. Geophys.*, *27*(11), 4257–4272, doi:10.5194/angeo-27-4257-2009.

Garrett, H. B., and A. C. Whittlesey (2000), Spacecraft charging, an update, *IEEE Trans. Plasma Sci.*, *28*(6), 2017–2028, doi:10.1109/27.902229.

Goertz, C. K. (1989), Dusty plasmas in the solar system, *Rev. Geophys.*, *27*(2), 271–292, doi:10.1029/RG027i002p00271.

Goldston, R. J., and P. H. Rutherford (1995), *Introduction to Plasma Physics IOP*, Cambridge University Press, Cambridge.

Grard, R. J. L. (1973), Properties of the Satellite Photoelectron Sheath Derived from

Photoemission Laboratory Measurements, *J. Geophys. Res.*, *78*(16), 2885–2906, doi:10.1029/JA078i016p02885.

Gudipati, M. S., R. Jacovi, I. Couturier-Tamburelli, A. Lignell, and M. Allen (2013), Photochemical activity of Titan's low-altitude condensed haze., *Nat. Commun.*, *4*(April), 1648, doi:10.1038/ncomms2649.

Gurnett, D. A. et al. (2004), The Cassini radio and plasma wave investigation, *Space Sci. Rev.*, *114*(1–4), 395–463, doi:10.1007/s11214-004-1434-0.

Havnes, O., L. I. Næsheim, T. W. Hartquist, G. E. Morfill, F. Melandsø, B. Schleicher, J. Trøim, T. Blix, and E. Thrane (1996), Meter-scale variations of the charge carried by mesospheric dust, *Planet. Space Sci.*, *44*(10), 1191–1194, doi:10.1016/S0032-0633(96)00041-4.

Hill, T. W. et al. (2012), Charged nanograins in the Enceladus plume, *J. Geophys. Res. Sp. Phys.*, *117*(5), n/a-n/a, doi:10.1029/2011JA017218.

Holmberg, M. K. G., J. E. Wahlund, M. W. Morooka, and A. M. Persoon (2012), Ion densities and velocities in the inner plasma torus of Saturn, *Planet. Space Sci.*, *73*(1), 151–160, doi:10.1016/j.pss.2012.09.016.

Horanyi, M., T. W. Hartquist, O. Havnes, D. a Mendis, and G. E. Morfill (2004), Dusty Plasma Effects in Saturn ' S Magnetosphere, *Reviews*, *42*(4), 1–20, doi:10.1029/2004RG000151.1.INTRODUCTION.

Hörst, S. M. et al. (2012), Formation of Amino Acids and Nucleotide Bases in a Titan Atmosphere Simulation Experiment, *Astrobiology*, *12*(9), 809–817, doi:10.1089/ast.2011.0623.

Hsu, H.-W., M. Horányi, and S. Kempf (2013), Dust and spacecraft charging in Saturn's E ring, *Earth, Planets Sp.*, *65*(3), 149–156, doi:10.5047/eps.2012.05.018.

Jacobsen, K. S., J. E. Wahlund, and A. Pedersen (2009), Cassini Langmuir probe measurements in the inner magnetosphere of Saturn, *Planet. Space Sci.*, *57*(1), 48–52, doi:10.1016/j.pss.2008.10.012.

Johnson, R. E., O. J. Tucker, M. Michael, E. C. Sittler, H. T. Smith, D. T. Young, and J. H. Waite (2010), Mass loss processes in titan's upper atmosphere, in *Titan from Cassini-Huygens*, pp. 373–391, Springer Netherlands, Dordrecht.

Kurth, W. S., T. F. Averkamp, D. A. Gurnett, and Z. Wang (2006), Cassini RPWS observations of dust in Saturn's E Ring, *Planet. Space Sci.*, *54*(9–10), 988–998, doi:10.1016/j.pss.2006.05.011.

Laframboise, J. G., and L. W. Parker (1973), Probe design for orbit-limited current collection, *Phys. Fluids*, *16*(5), 629, doi:10.1063/1.1694398.

Madanian, H., T. E. Cravens, M. S. Richard, J. H. Waite, N. J. T. Edberg, J. H. Westlake, and J. E. Wahlund (2016), Solar cycle variations in ion composition in the dayside ionosphere of Titan, *J. Geophys. Res. A Sp. Phys.*, *121*(8), 8013–8037, doi:10.1002/2015JA022274.

Mandt, K. E. et al. (2012), Ion densities and composition of Titan's upper atmosphere derived from the Cassini Ion Neutral Mass Spectrometer: Analysis methods and comparison of measured ion densities to photochemical model simulations, *J. Geophys. Res. E Planets*, *117*(10), E10006, doi:10.1029/2012JE004139.

Medicus, G. (1962), Spherical langmuir probe in Drifting'' and Accelerated'' maxwellian distribution, *J. Appl. Phys.*, *33*(10), 3094–3100, doi:10.1063/1.1728574.

Michael, M., S. N. Tripathi, P. Arya, A. Coates, A. Wellbrock, and D. T. Young (2011), High-altitude charged aerosols in the atmosphere of Titan, *Planet. Space Sci.*, *59*(9), 880–885, doi:10.1016/j.pss.2011.03.010.

Miller, S. L. (1953), A Production of Amino Acids Under Possible Primitive Earth Conditions, *Science (80-.).*, *117*(3046), 528–529, doi:10.1126/science.117.3046.528.

Mitchell, D. G. et al. (2009), Recurrent energization of plasma in the midnight-to-dawn quadrant of Saturn's magnetosphere, and its relationship to auroral UV and radio emissions, *Planet. Space Sci.*, *57*(14–15), 1732–1742, doi:10.1016/j.pss.2009.04.002.

Morooka, M. W. et al. (2009), The electron density of Saturn's magnetosphere, *Ann. Geophys.*, *27*(7), 2971–2991, doi:10.5194/angeo-27-2971-2009.

Morooka, M. W., J. E. Wahlund, A. I. Eriksson, W. M. Farrell, D. A. Gurnett, W. S. Kurth, A. M. Persoon, M. Shafiq, M. André, and M. K. G. Holmberg (2011), Dusty plasma in the vicinity of Enceladus, *J. Geophys. Res. Sp. Phys.*, *116*(12), A12221, doi:10.1029/2011JA017038.

Mott-Smith, H. M., and I. Langmuir (1926), The theory of collectors in gaseous discharges, *Phys. Rev.*, *28*(4), 727–763, doi:10.1103/PhysRev.28.727.

Müller-Wodarg, I. C. F., R. V. Yelle, J. Cui, and J. H. Waite (2008), Horizontal structures and dynamics of Titan's thermosphere, *J. Geophys. Res. E Planets*, *113*(10), E10005, doi:10.1029/2007JE003033.

Nagy, A. F. et al. (2004), The plasma environment of Mars, *Space Sci. Rev.*, *111*(1–2), 33–114, doi:10.1023/B:SPAC.0000032718.47512.92.

Niemann, H. B. et al. (2005), The abundances of constituents of Titan's atmosphere from the GCMS instrument on the Huygens probe, *Nature*, *438*(7069), 779–784, doi:10.1038/nature04122.

Pavlov, A. A., M. T. Hurtgen, J. F. Kasting, and M. A. Arthur (2003), Methane-rich proterozoic atmosphere?, *Geology*, *31*(1), 87–90, doi:10.1130/0091-7613(2003)031<0087:MRPA>2.0.CO;2.

Raulin, F., C. McKay, J. Lunine, and T. Owen (2009), Titan's Astrobiology, in *Titan from Cassini-Huygens*, pp. 215–233, Springer Netherlands, Dordrecht.

Richard, M. S. et al. (2015), An empirical approach to modeling ion production rates in Titan's ionosphere I: Ion production rates on the dayside and globally, *J. Geophys. Res. Sp. Phys.*, *120*(2), 1264–1280, doi:10.1002/2013JA019706.

Rosenqvist, L., J. E. Wahlund, K. Ågren, R. Modolo, H. J. Opgenoorth, D. Strobel, I. Müller-Wodarg, P. Garnier, and C. Bertucci (2009), Titan ionospheric conductivities from Cassini measurements, *Planet. Space Sci.*, *57*(14–15), 1828–1833, doi:10.1016/j.pss.2009.01.007.

Sagan, C., and B. Khare (1979), Tholins-organic chemistry of interstellar grains and gas, *Nature*, *277*(5692), 102–107, doi:10.1038/277102a0.

Sagan, C., B. N. Khare, W. R. Thompson, G. D. McDonald, M. R. Wing, J. L. Bada, T. Vo-Dinh, and E. T. Arakawa (1993), Polycyclic aromatic hydrocarbons in the atmospheres of Titan and Jupiter., *Astrophys. J.*, *414*(1), 399–405, doi:10.1086/173086.

Shukla, P. K. (2001), A survey of dusty plasma physics, *Phys. Plasmas*, *8*(5 II), 1791, doi:10.1063/1.1343087.

Shukla, P. K., and A. A. Mamun (2002), Introduction to Dusty Plasma Physics, *Plasma Phys. Control. Fusion*, *44*(3), 395–395, doi:10.1887/075030653X.

Sittler, E. C., A. Ali, J. F. Cooper, R. E. Hartle, R. E. Johnson, A. J. Coates, and D. T. Young (2009), Heavy ion formation in Titan's ionosphere: Magnetospheric introduction of free oxygen and a source of Titan's aerosols?, *Planet. Space Sci.*, *57*(13), 1547–1557, doi:10.1016/j.pss.2009.07.017.

Strobel, D. F., and J. Cui (2014), Titan's upper atmosphere/exosphere, escape processes, and rates, in *Titan*, edited by I. Muller-Wodarg, C. A. Griffith, E. Lellouch, and T. E. Cravens, pp. 355–375, Cambridge University Press, Cambridge.

Tarduno, J. A., R. D. Cottrell, M. K. Watkeys, A. Hofmann, P. V. Doubrovine, E. E. Mamajek, D. Liu, D. G. Sibeck, L. P. Neukirch, and Y. Usui (2010), Geodynamo, Solar Wind, and Magnetopause 3.4 to 3.45 Billion Years Ago, *Science (80-.).*, *327*(5970), 1238–1240, doi:10.1126/science.1183445.

Thissen, R., O. Witasse, O. Dutuit, C. S. Wedlund, G. Gronoff, and J. Lilensten (2011), Doubly-charged ions in the planetary ionospheres: a review, *Phys. Chem. Chem. Phys.*, *13*(41), 18264, doi:10.1039/c1cp21957j.

Thompson, W. R., G. D. McDonald, and C. Sagan (1994), The Titan haze revisited: Magnetospheric energy sources and quantitative tholin yield, *Icarus*, *112*(2), 376, doi:http://dx.doi.org/10.1006/icar.1994.1191.

Tian, F., S. C. Solomon, L. Qian, J. Lei, and R. G. Roble (2008), Hydrodynamic planetary thermosphere model: 2. Coupling of an electron transport/energy deposition model, *J. Geophys. Res. E Planets*, *113*(7), E07005, doi:10.1029/2007JE003043.

Tonks, L., and I. Langmuir (1929), Oscillations in ionized gases, *Phys. Rev.*, *33*(2), 195–210, doi:10.1103/PhysRev.33.195.

Vigren, E. et al. (2013), On the thermal electron balance in Titan's sunlit upper atmosphere, *Icarus*, *223*(1), 234–251, doi:10.1016/j.icarus.2012.12.010.

Vigren, E., M. Galand, O. Shebanits, J.-E. Wahlund, W. D. Geppert, P. Lavvas, V.

Vuitton, and R. V. Yelle (2014), Increasing Positive Ion Number Densities Below the Peak of Ion-Electron Pair Production in Titan'S Ionosphere, *Astrophys. J.*, *786*(1), 69, doi:10.1088/0004-637X/786/1/69.

Vigren, E. et al. (2015), Ionization balance in Titan's nightside ionosphere, *Icarus*, *248*, 539–546, doi:10.1016/j.icarus.2014.11.012.

Vuitton, V., P. Lavvas, R. V. Yelle, M. Galand, A. Wellbrock, G. R. Lewis, A. J. Coates, and J. E. Wahlund (2009), Negative ion chemistry in Titan's upper atmosphere, *Planet. Space Sci.*, *57*(13), 1558–1572, doi:10.1016/j.pss.2009.04.004.

Vuitton, V., O. Dutuit, M. A. Smith, and N. Balucani (2014), Chemistry of Titan's atmosphere, in *Titan*, edited by I. Muller-Wodarg, C. A. Griffith, E. Lellouch, and T. E. Cravens, pp. 224–284, Cambridge University Press, Cambridge.

Wahlund, J.-E. (2005), Cassini Measurements of Cold Plasma in the Ionosphere of Titan, *Science (80-.).*, *308*(5724), 986–989, doi:10.1126/science.1109807.

Wahlund, J.-E. et al. (2005), The inner magnetosphere of Saturn: Cassini RPWS cold plasma results from the first encounter, *Geophys. Res. Lett.*, *32*(20), L20S09, doi:10.1029/2005GL022699.

Wahlund, J.-E., R. Modolo, C. Bertucci, and A. J. Coates (2014), Titan's magnetospheric and plasma environment, in *Titan*, edited by I. Muller-Wodarg, C. A. Griffith, E. Lellouch, and T. E. Cravens, pp. 419–458, Cambridge University Press, Cambridge.

Wahlund, J. E. et al. (2009a), Detection of dusty plasma near the E-ring of Saturn, *Planet. Space Sci.*, *57*(14–15), 1795–1806, doi:10.1016/j.pss.2009.03.011.

Wahlund, J. E. et al. (2009b), On the amount of heavy molecular ions in Titan's ionosphere, *Planet. Space Sci.*, *57*(14–15), 1857–1865, doi:10.1016/j.pss.2009.07.014.

Waite, J. H., D. T. Young, T. E. Cravens, A. J. Coates, F. J. Crary, B. Magee, and J. Westlake (2007), The Process of Tholin Formation in Titan's Upper Atmosphere, *Science (80-.).*, *316*(5826), 870–875, doi:10.1126/science.1139727.

Waite, J. H., D. T. Young, J. H. Westlake, J. I. Lunine, C. P. McKay, and W. S. Lewis (2010), High-altitude production of titan's aerosols, in *Titan from Cassini-Huygens*, edited by R. H. Brown, J.-P. Lebreton, and J. H. Waite, pp. 201–214, Springer Netherlands, Dordrecht.

Wellbrock, A., A. J. Coates, G. H. Jones, G. R. Lewis, and J. H. Waite (2013), Cassini CAPS-ELS observations of negative ions in Titan's ionosphere: Trends of density with altitude, *Geophys. Res. Lett.*, *40*(17), 4481–4485, doi:10.1002/grl.50751.

Westlake, J. H., J. H. Waite, J. M. Bell, and R. Perryman (2014), Observed decline in Titan's thermospheric methane due to solar cycle drivers, *J. Geophys. Res. Sp. Phys.*, *119*(10), 8586–8599, doi:10.1002/2014JA020394.

Whipple, E. C. (1965), The equilibrium electric potential of a body in the upper atmosphere and in interplanetary space, George Washington University.

Whipple, E. C., T. G. Northrop, and D. A. Mendis (1985), The Electrostatics of a Dusty Plasma, *J. Geophys. Res.*, *90*(A8), 7405–7413, doi:10.1029/JA090iA08p07405.

Young, D. T. et al. (2004), Cassini plasma spectrometer investigation, *Space Sci. Rev.*, *114*(1–4), 1–112, doi:10.1007/s11214-004-1406-4.

Acta Universitatis Upsaliensis

Digital Comprehensive Summaries of Uppsala Dissertations from the Faculty of Science and Technology 1562

Editor: The Dean of the Faculty of Science and Technology

A doctoral dissertation from the Faculty of Science and Technology, Uppsala University, is usually a summary of a number of papers. A few copies of the complete dissertation are kept at major Swedish research libraries, while the summary alone is distributed internationally through the series Digital Comprehensive Summaries of Uppsala Dissertations from the Faculty of Science and Technology. (Prior to January, 2005, the series was published under the title "Comprehensive Summaries of Uppsala Dissertations from the Faculty of Science and Technology".)

Distribution: publications.uu.se
urn:nbn:se:uu:diva-329490

ACTA
UNIVERSITATIS
UPSALIENSIS
UPPSALA
2017